

# ELSA: Efficient LLM-Centric Split Aggregation for Privacy-Aware Hierarchical Federated Learning over the Network Edge

Xiaohong Yang, Tong Xie, Minghui Liwang, *Senior Member, IEEE*,  
Chikai Shang, Yang Lu, *Senior Member, IEEE*, Zhenzhen Jiao,  
Liqun Fu, *Senior Member, IEEE*, Seyyedali Hosseinalipour, *Senior Member, IEEE*

**Abstract**—Training large language models (LLMs) at the network edge faces fundamental challenges arising from device resource constraints, severe data heterogeneity, and heightened privacy risks. To address these challenges, we propose ELSA (Efficient LLM-centric Split Aggregation), a novel framework that systematically integrates split learning (SL) and hierarchical federated learning (HFL) for distributed LLM fine-tuning over resource-constrained edge networks. ELSA introduces three key innovations. First, it employs a task-agnostic, behavior-aware client clustering mechanism that constructs semantic fingerprints using public probe inputs and symmetric Kullback-Leibler (KL) divergence, augmented by prediction-consistency trust scoring and latency-aware edge assignment to jointly mitigate data heterogeneity, device unreliability, and communication constraints. Second, it employs a resource-aware dynamic model splitting strategy to adaptively partition the LLM into three segments across clients and edge servers, with the cloud used only for adapter aggregation, enabling an effective balance between on-device computation cost and global convergence stability. Third, it incorporates a lightweight communication scheme based on computational sketches combined with semantic subspace orthogonal perturbation (SS-OP) to reduce communication overhead while mitigating privacy leakage during model exchanges across the network. Extensive experiments across diverse NLP tasks demonstrate that ELSA consistently outperforms state-of-the-art baselines in terms of adaptability, convergence behavior, and robustness, establishing a scalable and privacy-aware solution for edge-side LLM fine-tuning under resource constraints.

**Index Terms**—Edge Computing, Hierarchical Federated Learning, Split Learning, LLM.

## I. INTRODUCTION

LARGE language models (LLMs) have demonstrated remarkable performance across a wide range of language understanding and generation tasks, motivating their rapid adoption in both research and real-world systems [1]–[3]. These models typically undergo a large-scale pre-training phase on centralized corpora to learn general language representations. This is followed by a fine-tuning phase that adapts the model to specific tasks, users, or environments, making fine-tuning the

Xiaohong Yang, Chikai Shang, Yang Lu and Liqun Fu are with the School of Informatics, Xiamen University, Fujian, China. Tong Xie is with the National University of Singapore. Minghui Liwang is with the Department of Control Science and Engineering, the National Key Laboratory of Autonomous Intelligent Unmanned Systems, and also with Frontiers Science Center for Intelligent Autonomous Systems, Ministry of Education, Tongji University, Shanghai, China. Zhenzhen Jiao is with the Teleinfo iF-Labs, China Academy of Information and Communications Technology. Seyyedali Hosseinalipour is with the Department of Electrical Engineering, University at Buffalo-SUNY, Buffalo, NY USA.

primary focus of LLM deployment at the network edge [4], [5]. Nevertheless, integrating LLM fine-tuning pipelines at the network edge faces fundamental limitations due to the constrained resources of edge devices, including compute, communication, memory, and energy. Compounding these constraints, data collected across edge devices is often highly skewed and non-independent and identically distributed (non-IID), which induces local model bias and degrades the performance of locally trained models. Together, these challenges highlight the need for a principled, architecture-aware distributed learning framework capable of enabling resource-efficient and robust LLM fine-tuning across edge devices [6]–[8].

Federated learning (FL) offers a natural solution to the aforementioned challenges by enabling collaborative model training across geo-distributed edge devices with non-IID data. In its conventional form, FL performs local model fine-tuning at edge devices, followed by periodic aggregation of model updates at a central server [9], [10]. However, as the scale of the system grows, requiring all edge devices to directly communicate with a single server can lead to severe congestion over backhaul links and impose substantial communication overhead. To alleviate this bottleneck, hierarchical federated learning (HFL) has emerged as an extension of FL, wherein edge devices communicate with intermediate aggregation nodes (e.g., edge servers or gateways), which perform partial model aggregation before forwarding model updates to a central server [11]–[13]. While HFL improves scalability and reduces backhaul load, it largely assumes that full model updates can still be locally obtained and transmitted, an assumption that becomes increasingly untenable for LLMs due to their massive parameter sizes and memory footprints. These limitations motivate the incorporation of split learning (SL), which partitions the model across devices and servers, enabling edge devices to train only lightweight model segments locally while offloading deeper, more resource-intensive components to computationally-capable network nodes (i.e., edge and cloud servers) [14], [15]. Although the combination of HFL and SL is particularly promising for scalable and resource-efficient LLM fine-tuning at the network edge, a principled framework that jointly integrates these two paradigms for LLMs remains largely unexplored, motivating this work.

Specifically, this work aims to systematically investigate the potential of jointly integrating SL and HFL for LLM fine-

TABLE I: Summary of related works on distributed LLM training and fine-tuning.

Reference	Research Field	Summary of Contribution
[16]	FL + Sentiment Analysis + LLM	Proposes a FL framework combining LLM with multi-scale CNN for sentiment analysis on COVID-19 social media data, enabling collaborative training across edge networks while preserving data privacy and improving communication efficiency through parameter aggregation.
[17]	FL + SL + LLM Pre-training	Introduces a federated SL approach for pre-training LLMs across distributed clients without sharing raw data, demonstrating effectiveness on GLUE tasks while maintaining privacy and reducing computational burden on resource-constrained devices.
[18]	FL + LLM + Network Security	Develops an efficient FL framework for malicious traffic detection by pre-training LLM on unlabeled network data and dynamically updating significant neurons, achieving superior detection performance while protecting critical infrastructure data privacy.
[19]	FL + LLM + Security	Integrates split FL with adaptive jamming defense for robust LLM training in adversarial wireless environments, enhancing privacy and resilience through multi-modal defense strategies combining differential privacy and beamforming.
[20]	Semantic Comm. + Fed-Split	Designs a knowledge-aware federated-split architecture for semantic communications, employing PPO with frozen LLM to optimize resource allocation, reducing training latency and improving semantic reconstruction accuracy.
[21]	IoT + SFL + Privacy	Develops a privacy-aware split FL scheme for IoT using Fisher information metrics, jointly optimizing split layer and resources to balance convergence speed, energy consumption, and privacy leakage.
[22]	SL + PEFT	Proposes the first SL framework for LLM fine-tuning combining federated parallel training with model splitting to significantly reduce client computational burden and enhance training efficiency.
[23]	Heterogeneous Devices + SL	Introduces a SL framework freezing device-side layers while centralizing LoRA fine-tuning on server, significantly reducing device computations and training time under data imbalance.
[24]	Wireless + Hierarchical SL	Proposes a hierarchical SL scheme with cloud-edge-user three-tier architecture, distributing model parts to reduce peak memory usage through parallel edge training and adapter aggregation.
[25]	Resource-Constrained + SFL	Develops a split FL framework for large AI models on edge devices, incorporating quantization and resource control to lower memory requirements and energy consumption while maintaining scalability.
[26]	Wireless + Split Fine-Tuning	Proposes a split fine-tuning scheme splitting LLM between edge server and devices with activation compression, optimizing resources to reduce fine-tuning delay and communication overhead significantly.
[27]	Vision + SL	Proposes a lightweight SL framework combining mask mechanism with differential privacy for large-scale vision pre-training in collaborative learning scenarios.
ELSA	Edge Intelligence + Dist. LLM	Integrates SL with HFL through three-part dynamic model partitioning across client-edge-cloud, incorporating behavior-aware clustering and computational sketches to balance computation cost with convergence stability and privacy.

tuning, forming a novel hybrid SL-HFL framework depicted in Fig. 1 that entails: (i) devising SL-driven model partitioning strategies that preserve the effectiveness and convergence of distributed LLM fine-tuning; (ii) developing mechanisms to address non-IID data distributions, client unreliability, and communication constraints in distributed LLM fine-tuning under SL-based model partitioning and HFL-style model aggregation; and (iii) mitigating privacy risks arising during training and model aggregation in hybrid SL-HFL settings, particularly those associated with data exposure or reconstruction through the observation of shared intermediate representations and model updates across the network. Key contributions of this work are summarized as follows:

- We propose ELSA (Efficient LLM-centric Split Aggregation), a framework that integrates SL and HFL to address device data heterogeneity and resource constraints for LLM fine-tuning at the network edge. Within ELSA, devices and edge servers collaboratively train edge-side model segments, while a cloud server performs global model aggregation.
- To enhance robustness under data heterogeneity, client unreliability, and communication constraints in distributed LLM fine-tuning, we design a task-agnostic, behavior-aware hierarchical clustering mechanism. This strategy is further enhanced with (i) a trustworthiness score based on prediction consistency (to filter poisoned or noisy clients), and (ii) a latency-aware edge

server assignment policy. In addition, we develop an SL-aware dynamic model segmentation strategy that explicitly leverages the heterogeneous capabilities of devices and edge servers, achieving a principled balance between training cost and model performance.

- To reduce communication overhead and improve system efficiency, we introduce a model compression scheme based on computational sketches. Building on this design, we incorporate semantic subspace orthogonal perturbation (SS-OP) to preserve data privacy throughout the training process, mitigating the risk of adversarial attacks and information leakage during model update exchanges across the network.
- Extensive evaluations on natural language processing (NLP) tasks, including text classification and information extraction, demonstrate that ELSA consistently outperforms state-of-the-art benchmarks, exhibiting superior model performance, convergence stability, and robustness under heterogeneous data and resource profiles of edge devices.

## II. LITERATURE REVIEW

### A. FL-driven Fine-Tuning of LLMs over the Network Edge

FL has been recently explored as a promising paradigm for LLM fine-tuning in network edge environments. For example, [28] introduced an adaptive asynchronous accelerated FL for LLMs to enhance resource utilization efficiency and model

accuracy in edge computing environments. [16] designed FL-empowered collaborative training for bidirectional encoder representations from transformers (BERT) models and multi-scale convolutional neural networks (CNNs). Also, [29] facilitated multi-user collaborative training of LLMs by integrating FL within model parallelism strategies, while [30] proposed a lightweight large-model-based joint multi-task multi-domain learning framework. Moreover, [18] presented an FL-driven LLM fine-tuning malicious traffic detection method using BERT, and [31] introduced a collaborative training framework for Transformer block classification based on FL.

Despite these contributions, existing FL-based LLM fine-tuning approaches largely overlook the fundamental scalability limitations that arise in large-scale edge networks. Specifically, as the number of participating devices grows, conventional FL architectures, where all devices directly communicate with a single aggregation server, suffer from severe communication congestion, backhaul link bottlenecks, and coordination overhead, issues that are further exacerbated by device data heterogeneity and limited resources. This implies that existing solutions relying on such flat topologies, such as [19]–[22], [25], may become ineffective or inefficient in large-scale scenarios due to these bottlenecks. These challenges naturally motivate HFL, which introduces intermediate aggregation points to improve scalability and communication efficiency. However, while HFL has shown promise in narrow-model settings [30], [32], [33], its application to LLM fine-tuning remains largely unexplored. Further, the massive parameter sizes and memory demands of LLMs introduce new constraints that require HFL architectures to be explicitly adapted to large-model training, a gap that this work aims to address through the integration of SL.

### B. Review of the Use of SL over the Network Edge

To address the challenges of LLM fine-tuning at the network edge under device resource constraints, two prevalent strategies are commonly adopted: (i) fine-tuning only a subset of LLM parameters using parameter-efficient methods such as low-rank adaptation (LoRA); and (ii) partitioning the model into multiple segments and distributing the training process across multiple computing nodes. Both strategies have recently attracted significant attention in the literature. For instance, [34] proposed to partition the LLM into two segments for client-server collaborative training. [23] proposed a fine-tuning framework for LLMs by strategically partitioning LLMs into device-side frozen layers and server-side, LoRA-enabled fine-tuning layers. [27] introduced a lightweight mask-based segmentation learning framework for the collaborative fine-tuning of LLMs. [35] presented a distributed hybrid federated segmentation learning framework that leverages device-to-device communications to aggregate edge resources for model training. [17] designed a segmented learning framework to facilitate the collaborative training of BERT models.

Although the above studies have advanced LLM fine-tuning, they have largely neglected the communication costs incurred during conventional FL: they do not consider LLM fine-tuning under HFL architectures, which entail a better scalability and

backhaul link load. However, even with the integration of HFL and SL, fundamental challenges inherited from conventional FL scenarios (e.g., severe data heterogeneity, client device heterogeneity, and network dynamics) persist and are further amplified in the LLM fine-tuning context due to larger model sizes and more complex semantic representations. Existing works, including [23], [24], [26], [27], often overlook such issues. In addition, privacy vulnerabilities arising from the joint use of HFL and SL in LLM fine-tuning, particularly those related to information leakage through shared model updates, remain largely unexplored. These gaps motivate our focus on developing a unified framework that jointly addresses model scalability, data heterogeneity, and privacy preservation for LLM fine-tuning at the edge.

We finally note that existing distributed LLM fine-tuning frameworks primarily reason about data heterogeneity but often overlook model behavioral heterogeneity. In LLMs, this distinction is crucial: two clients may hold similar data yet learn fundamentally different semantic representations. As summarized in Table I, ELSA introduces a semantics-centric framework that directly addresses this gap. Through task-agnostic probing, we quantify how local models interpret the same inputs, enabling behavior-aware client clustering beyond label statistics. Combined with resource-adaptive model splitting and privacy-preserving sketching, ELSA unifies semantic alignment, resource efficiency, and privacy into a single coherent design.

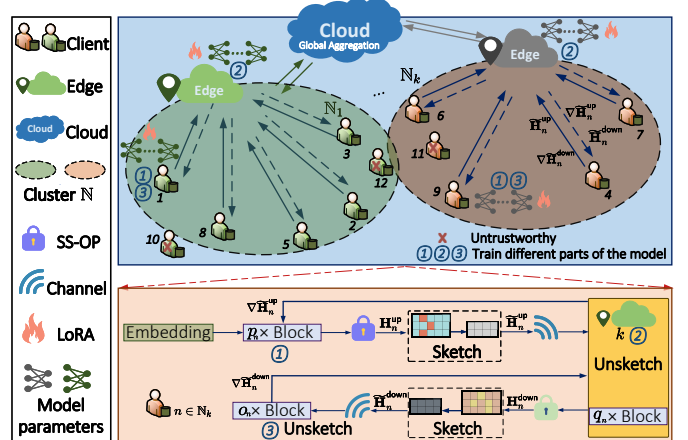


Fig. 1: A schematic of our proposed ELSA: clients and edge servers collaboratively fine-tuning LLMs via LoRA, with activations compressed during transmission; the cloud globally aggregates the LoRA parameters.

## III. PROPOSED METHOD

### A. Problem Formulation

We consider distributed learning through an HFL architecture, where the system consists of a cloud server, multiple edge servers  $\mathcal{K} = \{1, \dots, k, \dots, K\}$ , and a set of clients  $\mathcal{N} = \{1, \dots, n, \dots, N\}$ , as illustrated in the upper right portion of Fig. 1. Each client  $n$  owns a local dataset  $\mathcal{D}_n = \{(\mathbf{x}_j, y_j) | 1 \leq j \leq |\mathcal{D}_n|\}$ , where  $\mathbf{x}_j$  and  $y_j$  refer to the feature vector and the label of the  $j^{\text{th}}$  local data point, respectively. Subsequently, given a pre-trained LLM with frozen backbone parameters  $w^{\text{LLM}}$  and

the trainable fine-tuning parameter  $\theta$ , the loss function for a data sample  $(\mathbf{x}_j, y_j)$  is defined via the task specific loss (e.g., cross entropy for classification):

$$f(\mathbf{x}_j, y_j; w^{\text{LLM}}, \theta) = \mathcal{L}_{\text{task}}(s(\mathbf{x}_j; w^{\text{LLM}}, \theta), y_j) \quad (1)$$

where  $s(\cdot)$  is the LLM’s representation output. Collectively, the optimization objective of our interest is to minimize the global loss function across all participating clients, defined as:

$$\operatorname{argmin}_{\theta} \tilde{F}(\theta) = \sum_{n=1}^N \frac{|\mathcal{D}_n|}{|\mathcal{D}|} F_n(\theta), \quad (2)$$

where  $|\mathcal{D}| = \sum_{n=1}^N |\mathcal{D}_n|$ , and

$$F_n(\theta) = \frac{1}{|\mathcal{D}_n|} \sum_{(\mathbf{x}_j, y_j) \in \mathcal{D}_n} f(\mathbf{x}_j, y_j; w^{\text{LLM}}, \theta). \quad (3)$$

To tackle the optimization objective in (2), we propose **ELSA**, a HFL framework tailored for distributed LLM fine-tuning under resource and privacy constraints. ELSA systematically addresses three core challenges: (i) semantic heterogeneity across clients via behavior-aware clustering, (ii) communication overhead and label leakage via tripartite split training with layered compression, and (iii) robust global aggregation via trust-weighted fusion at the cloud level. An overview of ELSA is presented in Alg. 1, and the following subsections elaborate on each technical component in detail.

### B. Learning Architecture of ELSA

In the following, we first introduce a client clustering strategy based on Kullback–Leibler divergence (KLD) to address data heterogeneity and unreliable trustworthiness and communications across clients. Then, we detail the end-to-end workflow of LLM partitioning and collaborative training across clients. Finally, we present a compression framework aimed at simultaneously enhancing communication efficiency and safeguarding the data privacy during the training.

1) *Behavior-aware Hierarchical Clustering and Robust Aggregation*: Existing studies in FL, including HFL, have widely adopted KLD to cluster clients based on their label distributions [36], [37], under the assumption that clients with similar categorical proportions exhibit compatible optimization landscapes, particularly in vision tasks using narrow-models such as CNNs. While effective in label-rich settings, this approach fundamentally fails to capture the unique characteristics of distributed LLM fine-tuning, where: (i) downstream tasks (e.g., classification, extractive summarization, or sequence labeling) do not share a universal label space, making label-proportion-based clustering inapplicable; (ii) data heterogeneity manifests not merely in class frequencies, but in semantic and behavioral discrepancies (i.e., how local LLMs interpret and respond to the same linguistic input).

Moreover, real-world HFL deployments face two critical yet often overlooked challenges: unreliable clients (due to data poisoning or label noise) and unstable connectivity (especially for geographically distant clients). Traditional KLD-based clustering [36], [37], by focusing solely on static label statistics, provides no mechanism to account for these system-level

constraints. To bridge this gap, we propose a task-agnostic behavioral profiling framework that extends conventional notions of device similarity beyond label distributions by quantifying semantic behavioral divergence, wherein distinct local models are identified through their differing predictive logic when exposed to the same inputs. To achieve this, our framework is built upon three pillars:

- A probe-based behavioral fingerprint derived from public inputs, enabling KLD-driven clustering without assuming task type or label space of clients;
- A trustworthiness score grounded in prediction consistency to down-weight clients with polluted or anomalous data;
- A client-to-server assignment policy that respects physical network constraints between clients and edge servers.

Subsequently, we formalize our approach in four steps:

**Step 1: Construction of a Public Probe Set.** We construct a lightweight, public probe dataset  $\mathcal{P} = \{x^{(1)}, \dots, x^{(Q)}\}$  by sampling diverse inputs from open benchmarks (e.g., GLUE, TREC, or SQuAD development datasets [38], [39]). This set is distributed by the cloud server to all clients and serves as a common reference for behavioral evaluation, without exposing any private data.

**Step 2: Task-Agnostic Behavioral Fingerprint Extraction.** For each client  $n$ , we feed every probe input  $x^{(j)} \in \mathcal{P}$  into its locally fine-tuned LLM (e.g., BERT) and extract the contextual representation of the [CLS] token, a standard sentence-level embedding used across transformer-based LLMs, denoted by  $\mathbf{T}_n^j \in \mathbb{R}^{\text{D}^{\text{hidden}}}$ , where  $\text{D}^{\text{hidden}}$  represents the hidden layer dimension. To obtain a unified-dimension, task-agnostic profile that is invariant to downstream task head structures, we model the client’s behavioral fingerprint as a multivariate Gaussian distribution:

$$R_n = \tilde{\mathcal{N}}(\boldsymbol{\mu}_n, \boldsymbol{\Sigma}_n), \quad (4)$$

where  $\boldsymbol{\mu}_n = \frac{1}{Q} \sum_{j=1}^Q \mathbf{T}_n^{(j)}$  represents the average semantic representation of the [CLS] vector for client  $n$  across all probe samples and  $\boldsymbol{\Sigma}_n = \frac{1}{Q} \sum_{j=1}^Q (\mathbf{T}_n^{(j)} - \boldsymbol{\mu}_n)(\mathbf{T}_n^{(j)} - \boldsymbol{\mu}_n)^\top$  captures the dispersion of the [CLS] vectors of client  $n$  around its mean.

**Step 3: Symmetric KLD for Behavioral Discrepancy.** We quantify the data heterogeneity between clients  $n$  and  $n'$  via the symmetrized KLD between their Gaussian fingerprints:

$$\mathcal{R}(n, n') = \text{KL}(R_n \| R_{n'}) + \text{KL}(R_{n'} \| R_n), \quad (5)$$

where the closed-form KLD between multivariate Gaussians is given by

$$\begin{aligned} \text{KL}(\tilde{\mathcal{N}}_n \| \tilde{\mathcal{N}}_{n'}) &= \frac{1}{2} \left[ \text{tr}(\boldsymbol{\Sigma}_{n'}^{-1} \boldsymbol{\Sigma}_n) - \text{D}^{\text{hidden}} + \ln \frac{|\boldsymbol{\Sigma}_{n'}|}{|\boldsymbol{\Sigma}_n|} \right. \\ &\quad \left. + (\boldsymbol{\mu}_{n'} - \boldsymbol{\mu}_n)^\top \boldsymbol{\Sigma}_{n'}^{-1} (\boldsymbol{\mu}_{n'} - \boldsymbol{\mu}_n) \right]. \end{aligned} \quad (6)$$

This yields an  $N \times N$  behavioral distance matrix that reflects semantic divergence beyond label statistics across clients.

**Step 4: Trust and Communication-Aware Client Clustering.** To ensure robustness against data pollution and practical deployability under network constraints, we integrate

trustworthiness and communication feasibility into a unified client clustering framework. Specifically, we first compute a *trustworthiness score* for each client  $n$  as follows:

$$w_n^{\text{trust}} = \exp \left( \underbrace{-\frac{1}{Q} \sum_{j=1}^Q \frac{1}{\|\mathbf{T}_n^{(j)}\|_2}}_{\text{inverse confidence}} - \underbrace{\frac{1}{N-1} \sum_{n' \neq n} \mathcal{R}(n, n')}_{\text{mean behavioral divergence } \bar{\mathcal{R}}_n} \right),$$

where  $\frac{1}{\|\mathbf{T}_n^{(j)}\|_2}$  is the inverse confidence of its [CLS] embeddings across the public probe set  $\mathcal{P}$ . Intuitively, a client with low prediction entropy (high confidence) and low divergence from peers (consistent behavior) receives a high trust score. We then define the *communication-feasible edge server set* for each client  $n$  as:

$$\mathcal{E}_n = \{k \mid \tau_{n,k} \leq \tau_{\max}, k \in \mathcal{K}\},$$

where  $\tau_{n,k}$  is the round-trip latency between client  $n$  and edge server  $k$ , and  $\tau_{\max}$  is a system-defined threshold (e.g., 200 ms). We finally construct a *communication-constrained client partition* through a four-stage process.

**(Stage 1)** For each edge server  $k$ , we define its candidate client set as  $\mathcal{C}_k = \{n \mid k \in \mathcal{E}_n\}$ .

**(Stage 2)** We perform spectral clustering *independently within each  $\mathcal{C}_k$* , using a trust-weighted affinity matrix  $\mathbf{A}^{(k)}$  with entries:

$$\mathbf{A}_{n,n'}^{(k)} = w_n^{\text{trust}} \cdot w_{n'}^{\text{trust}} \cdot \exp(-\gamma \cdot \mathcal{R}(n, n')), \quad \forall n, n' \in \mathcal{C}_k,$$

where  $\gamma > 0$  controls the sensitivity to behavioral divergence.

**(Stage 3)** For each resulting cluster  $\mathbb{N}_k \subseteq \mathcal{C}_k$ , we compute its average trust score  $\bar{w}_k^{\text{trust}} = \frac{1}{|\mathbb{N}_k|} \sum_{n \in \mathbb{N}_k} w_n^{\text{trust}}$ .

**(Stage 4)** If  $\bar{w}_k < w_{\min}$  (a trust threshold), we either: (i) merge  $\mathbb{N}_k$  into the nearest high-trust cluster (measured by centroid KLD), or (ii) escalate it to cloud-level aggregation if no suitable merge target exists.

The final grouping  $\{\mathbb{N}_k\}_{k=1}^K$  ensures that each cluster: (i) consists of behaviorally similar clients, (ii) excludes or mitigates the influence of polluted data, and (iii) is assigned to an edge server with reliable connectivity, thereby enabling stable, efficient, and deployable hierarchical model aggregation.

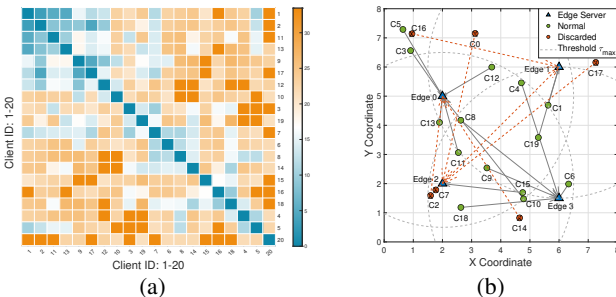


Fig. 2: Client behavioral heterogeneity and clustering outcome in a 20-client network. Left:  $20 \times 20$  pairwise KLD matrix  $\mathcal{R}(n, n')$  across all clients. Right: final client-server association mapping.

To facilitate understanding, in Fig. 2, we consider a network with 20 clients, where each client’s local dataset is constructed by partitioning the SQuAD dataset using Dirichlet distribution with concentration parameter  $\hat{\alpha} = 0.1$ . Fig. 2(a) provides a heatmap of pairwise KLD ( $\mathcal{R}(n, n')$ ) to visualize data distribution variations, while Fig. 2(b) illustrates the final client clustering (i.e., client-to-server association) results. Across all edge server groups, clients marked with ‘X’ are either out-of-range or deemed untrustworthy; only high-trust, in-range clients participate in edge-level aggregation, specifically those shown as green circles labeled ‘Normal’.

**2) Model Splitting and Collaborative Training:** The tripartite model segmentation in ELSA, where both the initial (Part 1) and final (Part 3) segments reside on the client, while the intermediate transformer blocks (Part 2) are offloaded to the server, is deliberately designed to address two critical challenges in edge-based LLM fine-tuning: *privacy preservation* and *label confidentiality*. This design follows a principled insight for LLMs: by retaining the output layer (e.g., task-specific head) on the client side, the ground-truth labels never leave the local device, thereby eliminating the risk of label leakage during training. Moreover, keeping both input embedding and output layers locally prevents the server from directly accessing raw embedding gradients or logits, which are known to be highly susceptible to reconstruction attacks. Consequently, this symmetric client-side placement ensures that sensitive user data, including input tokens, labels, and final predictions, remain strictly within the trusted execution environment of the client, while only intermediate hidden states (obfuscated via SS-OP and sketching, as detailed in later) are exchanged with the server.

Building upon this privacy-aware architecture, we integrate SL into our HFL framework, as illustrated in Fig. 1 and Fig. 3. Specifically, in Fig. 3, we consider the LLM architecture (e.g., BERT) as  $\mathcal{M}$  transformer blocks stacked in series, and unlike static partitioning, we employ a *resource-aware dynamic splitting strategy* to determine the number of layers for each segment adaptively for each client  $n$ . The first segment comprises an embedding layer and  $p_n$  transformer blocks (Part 1), each of which includes multi-head attention modules, feed-forward networks (FFNs), and related components (e.g., residual connections and layer normalization). The second segment consists of  $q_n$  transformer blocks (Part 2), and the third segment contains  $o_n$  transformer blocks along with the output layer (Part 3). The first and third segments are deployed on the client-side, while the second segment can be placed on the corresponding server-side. Specifically, each attention module within Parts 1–3 is augmented with trainable low-rank matrices  $\theta = [\theta_1, \theta_2, \theta_3]$  (i.e.,  $\theta = \{(A_i^m, B_i^m) \mid i \in \{1, 2, 3\}, m \in \{1, \dots, \mathcal{M}\}\}$ ) forming the adapters, where  $\theta \in \mathbb{R}^M$  ( $M \ll D$ ), and the output layer in Part 3 is also trainable but contributes negligibly to total parameter count.

To balance computational load and communication costs, the offloading ratio is determined by the client’s available computational capacity  $\mathcal{H}_n$  (e.g., FLOPS) and uplink bandwidth  $\mathcal{B}_n$ .

We define the *offloading preference score*  $\mathcal{G}_n$  for client  $n$  as:

$$\mathcal{G}_n = \lambda_1 \cdot \left(1 - \frac{\mathcal{H}_n}{\mathcal{H}_{\max}}\right) + \lambda_2 \cdot \frac{\mathcal{B}_n}{\mathcal{B}_{\max}}, \quad (7)$$

where  $\mathcal{H}_{\max}$  and  $\mathcal{B}_{\max}$  (in bytes/second) are the maximum observed capacity and bandwidth in the system, and  $\lambda_1, \lambda_2$  are weighting factors ( $\lambda_1 + \lambda_2 = 1$ ).

Unlike symmetric partitioning, we fix the depth of the output segment to  $o_n = o_{\text{fix}}$  (e.g.,  $o_{\text{fix}} = 2$ ) for all clients. This design ensures that the task-specific head remains strictly local for label privacy and maintains a consistent model structure across the federation. Consequently, the dynamic adjustment focuses on balancing the local encoder depth  $p_n$  and the offloaded encoder depth  $q_n$ . To prevent the local feature extractor from becoming overly specialized to non-IID data (a phenomenon known as over-personalization), we constrain the local encoder layers within a safe range  $[p_{\min}, p_{\max}]$ . The number of offloaded layers  $q_n$  is then dynamically calculated as:

$$q_n = \mathcal{M} - o_{\text{fix}} - p_n, \quad (8)$$

where the local encoder depth  $p_n$  is determined by mapping the preference score  $\mathcal{G}_n$  to the valid range:

$$p_n = p_{\max} - \lfloor \mathcal{G}_n \cdot (p_{\max} - p_{\min}) \rfloor. \quad (9)$$

Here,  $p_{\min}$  (e.g., 1) guarantees basic input embedding privacy, while  $p_{\max}$  serves as a theoretical upper bound to safeguard global model generalization. This dynamic mechanism ensures that clients with limited computational resources or high-quality connections offload more work to the edge, while powerful clients or those with poor connectivity perform more local computation. In essence, the rationale for this partitioning is rooted in the client's limited computational resources, the requirement for decision-making autonomy, and the necessity for end-to-end privacy control.

Each client  $n \in \mathbb{N}_k$  within the coverage edge server  $k$ , forwards its data through Part 1 of its model, generating a hidden layer state, defined as

$$\mathbf{H}_n^{\text{up}} = \left[ h_{n,1}^{\text{up}}, \dots, h_{n,d}^{\text{up}}, \dots, h_{n,D}^{\text{up}} \right] \in \mathbb{R}^{\text{D}} \Big|_{f_{\text{embed}}(x; \theta_1) \rightarrow f_{1 \sim p_n}}, \quad (10)$$

where  $h_{n,d}^{\text{up}}$  is the  $d$ -th component of  $\mathbf{H}_n^{\text{up}}$ ,  $f_{\text{embed}}(x)$  denotes the embedding layer of the LLM, and  $f_{1 \sim p_n}$  represents the sequential feed-forward through transformer block 1 to block  $p_n$  at the client. The client then aims to send this hidden layer state to the edge server to continue the process of model fine-tuning. However, since the direct transmission of the hidden layer state  $\mathbf{H}_n^{\text{up}}$  can lead to privacy leakage (e.g., through model inversion attacks) and incur excessive communication overhead, the client first compresses its hidden layer state using a sketch-based method (Section B.3) and then uploads both compressed representation and the attention mask  $\mathcal{A}_n$  to the edge server. Once the information is received, the edge server will decompress it to obtain an approximate information  $\tilde{\mathbf{H}}_n^{\text{up}}$  of  $\mathbf{H}_n^{\text{up}}$ . Then, the edge server uses  $\tilde{\mathbf{H}}_n^{\text{up}}$  and  $\mathcal{A}_n$  as inputs to perform the computationally intensive operations, yielding the hidden state  $\mathbf{H}_n^{\text{down}}$ , defined as

$$\mathbf{H}_n^{\text{down}} = \left[ h_{n,1}^{\text{down}}, \dots, h_{n,d}^{\text{down}}, \dots, h_{n,D}^{\text{down}} \right] \in \mathbb{R}^{\text{D}} \Big|_{f_{p_n+1 \sim p_n+q_n}(\tilde{\mathbf{H}}_n^{\text{up}}, \mathcal{A}_n; \theta_2)}, \quad (11)$$

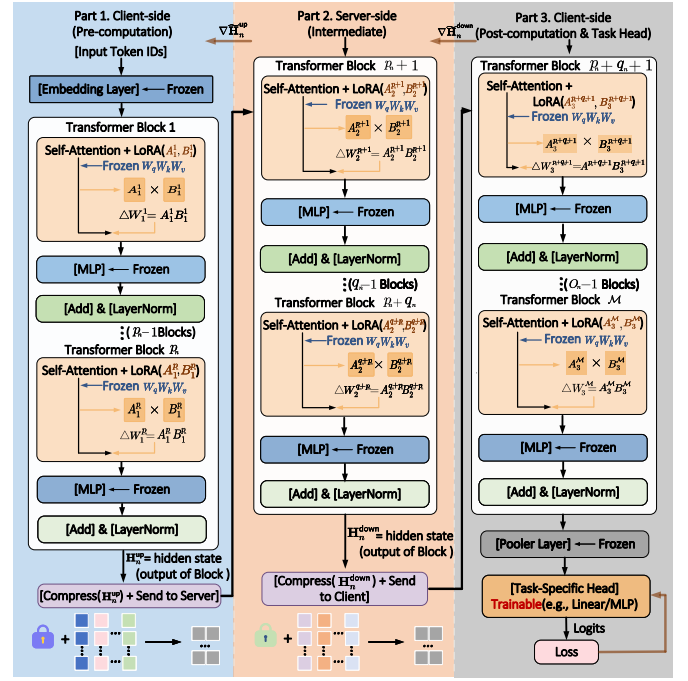


Fig. 3: Breakdown of ELSA: client trains Part 1, sends compressed activations to edge for Part 2, which then feeds into Part 3 on client. Gradients flow backward symmetrically ( $\nabla \tilde{\mathbf{H}}_n^{\text{down}} \rightarrow \text{Edge}$ ,  $\nabla \mathbf{H}_n^{\text{up}} \rightarrow \text{Client}$ ), completing one round.

where  $h_{n,d}^{\text{down}}$  is the  $d$ -th component of  $\mathbf{H}_n^{\text{down}}$  and  $f_{p+1 \sim p+q}(\cdot)$  denotes sequential feed-forward through transformer blocks  $p_n$  to  $p_n + q_n$ . Then,  $\mathbf{H}_n^{\text{down}}$  will be compressed into  $\tilde{\mathbf{H}}_n^{\text{down}}$  and then sent to the client.

Finally, the latest  $o_n$  model segments on the client-side perform computations to obtain the logits  $\mathcal{Z}$  and the loss value, which triggers gradient backpropagation; mathematically,

$$\mathcal{Z} = f_{p_n+q_n+1 \sim \mathcal{M}}(\tilde{\mathbf{H}}_n^{\text{down}}, \mathcal{A}_n; \theta_3), \quad (12)$$

$$\mathbb{L} = \mathcal{F}_{\text{loss}}(f_{\text{out}}(\mathcal{Z}, y)), \quad (13)$$

where  $f_{p_n+q_n+1 \sim \mathcal{M}}(\cdot)$  denotes sequential feed-forward through transformer blocks  $p_n + q_n$  to  $p_n + q_n + o_n$ ,  $f_{\text{out}}(\cdot)$  is the output layer of the model,  $y$  is the targeting sentences and  $\mathcal{F}_{\text{loss}}(\cdot)$  denotes the loss function.

After computing the loss, each client performs gradient backpropagation locally to update Blocks  $o$ , then transmits the gradient of hidden states  $\tilde{\mathbf{H}}_n^{\text{down}}$  back to the server (i.e.,  $\nabla \tilde{\mathbf{H}}_n^{\text{down}}$ ). The server executes gradient backpropagation on Blocks  $q$ , updates its parameters, and subsequently transmits the gradients of hidden states  $\mathbf{H}_n^{\text{up}}$  back to the client. Lastly, Blocks  $p$  perform gradient backpropagation, which completes a training round.

While client-edge collaboration improves training efficiency, the restricted representational power of isolated local updates can compromise global model expressiveness. To mitigate this, we periodically aggregate model parameters at the cloud: after every fixed number of collaborative training rounds (i.e.,  $t$ ), each edge server  $k$  uploads its locally refined adapter parameters to the cloud server for global model aggregation.

Consistent with our behavior-aware clustering and robustness-oriented design, the contribution of each edge server to the global aggregation is weighted according to two factors: (i) the internal behavioral coherence of its client group, and (ii) the aggregated trustworthiness of the participating clients. Specifically, we define:

$$\alpha_k = \frac{1}{1 + \overline{\mathcal{R}}_k} \times \bar{w}_k^{\text{trust}}, \quad (14)$$

where  $\overline{\mathcal{R}}_k = \frac{1}{\lfloor \mathbb{N}_k \rfloor (\lfloor \mathbb{N}_k \rfloor - 1)} \sum_{n \neq n' \in \mathbb{N}_k} \mathcal{R}(n, n')$  is the average pairwise symmetric KLD among clients in group  $\mathbb{N}_k$ . Next, we obtain the normalized weights  $\tilde{\alpha}_k = \frac{\alpha_k}{\sum_{k=1}^K \alpha_k}$ , using which we obtain the global model  $\theta_g$ , as follows:

$$\theta_g = \sum_{k=1}^K \tilde{\alpha}_k \theta_{g,k}, \quad (15)$$

where  $\theta_{g,k}$  represents adapter parameters obtained through collaborative training between edge server  $k$  and clients within its coverage area during the  $g^{\text{th}}$  global iteration. Further, we consider that the training ends at global aggregation once two consecutive global models satisfy the following condition:

$$\|\theta_g - \theta_{g-1}\|_2 \leq \xi, \quad (16)$$

where  $\xi$  is a small positive value used to control the convergence criterion.

3) *Layered Compression for Secure and Efficient Communications*: To simultaneously reduce communication overhead and mitigate the privacy leakage during the information exchange between clients and edge servers, we design a layered compression-and-obfuscation mechanism based on computational sketches, which is tailored to preserve semantic fidelity in NLP model updates. Specifically, we propose a *semantic subspace orthogonal perturbation* (SS-OP) mechanism, wherein instead of applying a single global orthogonal transform, each client  $n$  focuses on the dominant semantic subspace from its local hidden activations. Specifically, let  $\mathbf{J}_n \in \mathbb{R}^{\mathbf{Q} \times \mathbf{D}^{\text{hidden}}}$  denote the matrix of  $\mathbf{Q}$  hidden states (e.g., [CLS] vectors) collected over a recent batch of probe or training inputs. Client  $n$  computes the top- $r$  principal components via truncated singular value decomposition (or power iteration):

$$\mathbf{U}_n = \text{Top}_r(\text{SVD}(\mathbf{J}_n)) \in \mathbb{R}^{\mathbf{D}^{\text{hidden}} \times r}, \quad (17)$$

where  $\mathbf{U}_n^\top \mathbf{U}_n = \mathbf{I}_r$  spans the most informative semantic directions. Next, a client-specific random orthogonal matrix  $\mathbf{V}_n \in \mathbb{R}^{r \times r}$  is generated by QR decomposition of a pseudo-random Gaussian matrix seeded from the client ID and a pre-shared salt:

$$\mathbf{V}_n = \text{QR}(\Phi(n)), \quad (18)$$

where  $[\Phi(n)]_{i,j} \sim \tilde{\mathcal{N}}(0, 1)$  with  $\text{seed}_n = \text{Hash}(s \parallel n)$ , and  $s$  is a pre-shared salt value. The full perturbation matrix is then constructed as:

$$\mathbf{Q}_n = \mathbf{U}_n \mathbf{V}_n \mathbf{U}_n^\top + (\mathbf{I}_{\mathbf{D}^{\text{hidden}}} - \mathbf{U}_n \mathbf{U}_n^\top). \quad (19)$$

---

### Algorithm 1: Overview of ELSA: Efficient LLM-centric Split Aggregation

---

**Input** : Client set  $\mathcal{N}$ , Edge server set  $\mathcal{K}$ , Public probe set  $\mathcal{P}$ , Pre-trained LLM  $w^{\text{LLM}}$ , Local rounds  $t$ .  
**Output**: Global optimized parameters  $\theta_g$ .

- 1 **Initialization**:  $w_n^{\text{trust}} = 0$ ,  $\mathcal{E}_n = \emptyset$ .
- 2 **Phase 1: Behavior-aware Client Clustering**
  - 3 1.1 *Behavioral Fingerprinting*: Each client  $n$  computes Gaussian fingerprint  $R_n = \tilde{\mathcal{N}}(\boldsymbol{\mu}_n, \Sigma_n)$  using probe set  $\mathcal{P}$ ;
  - 4 1.2 *Discrepancy Measurement*: Compute symmetric KL divergence matrix  $\mathcal{R}(n, n')$  between all client pairs;
  - 5 1.3 *Trust & Assignment*: Calculate trust score  $w_n^{\text{trust}}$  and communication feasibility  $\mathcal{E}_n$ . Perform spectral clustering within feasible edge groups to obtain clusters  $\{\mathbb{N}_k\}_{k=1}^K$ ;
- 6 **Phase 2: Collaborative Training & Aggregation**
- 7 **if** The global model parameter  $\theta_g$  changes does not satisfy (16) **then**
  - 8 **foreach** edge server  $k \in \mathcal{K}$  **do**
    - 9 **for**  $t = 1$  **to**  $t$  **do**
      - 10 **foreach** client  $n \in \mathbb{N}_k$  **do**
        - 11 *Forward Pass (Split)*: Client computes Part 1 output  $\mathbf{H}_n^{\text{up}}$ ;
        - 12 *Compression & Privacy*: Apply SS-OP and sketching to generate  $\tilde{\mathbf{H}}_n^{\text{up}}$ . Upload to Edge  $k$ ;
        - 13 *Edge Processing*: Edge computes Part 2 output  $\mathbf{H}_n^{\text{down}}$  using  $\tilde{\mathbf{H}}_n^{\text{up}}$ . Compress and send back  $\tilde{\mathbf{H}}_n^{\text{down}}$ ;
        - 14 *Client Completion*: Client computes Part 3 output, calculates loss  $\mathbb{L}$ , and initiates backpropagation;
        - 15 *Backward Pass*: Gradients flow symmetrically: Client (Part 3)  $\rightarrow$  Edge (Part 2)  $\rightarrow$  Client (Part 1);
      - 16 Edge  $k$  aggregates local adapter parameters to obtain  $\theta_{g,k}$ ;
    - 17 **Phase 3: Cloud-level Global Aggregation**
    - 18 Compute edge weights  $\alpha_k = \frac{1}{1 + \overline{\mathcal{R}}_k} \times \bar{w}_k^{\text{trust}}$ ;
    - 19 Normalize weights  $\tilde{\alpha}_k$  and update global model:  $\theta_g = \sum_{k=1}^K \tilde{\alpha}_k \theta_{g,k}$ ;
    - 20 **return**  $\theta_g$ ;

---

This matrix is orthogonal ( $\mathbf{Q}_n^\top \mathbf{Q}_n = \mathbf{I}_{\mathbf{D}^{\text{hidden}}}$ ) and performs a random rotation *only within the semantic subspace*, leaving the orthogonal complement unchanged. This design ensures that:

(1) **Privacy is strengthened**: Adversaries cannot recover the original semantics without knowing both  $\mathbf{U}_n$  (data-dependent) and  $\mathbf{V}_n$  (secret-seeded).

(2) **Training remains stable**: During backpropagation, the client applies  $\mathbf{Q}_n^\top$  to restore exact gradients, as  $\mathbf{Q}_n$  is orthogonal.

(3) **Activation structure is preserved**: Zero or low-magnitude dimensions outside the semantic subspace remain unaltered, maintaining compatibility with downstream layers (e.g., attention heads or classification heads).

The uploaded hidden state is then computed as  $\tilde{\mathbf{H}}_n = \mathbf{Q}_n \mathbf{H}_n$ , which is compressed into a  $Y \times Z$  sketch matrix  $\mathbf{U}$  using  $Y$  independent hash functions, where  $Z \ll \mathbf{D}$ .

Specifically, each sketch element is calculated as:

$$U_{n,[j,k]} = \sum_{d:h_{n,j}(d)=u} \text{sign}_j(d) \cdot h_{n,d}^{\text{up}}, \quad (20)$$

where  $u \in \{1, 2, \dots, Z\}$  represents the column index of sketch matrix  $U$  and  $\text{sign}_{j:1 \leq j \leq Y} : \mathcal{D} \rightarrow \{+1, -1\}$  denotes  $Y$  pairwise independent sign hash functions. Besides, we define the compression ratio throughout the entire transmission process as  $\rho = \mathcal{D}/(YZ)$ .

At the edge, we recover the original hidden layer information based on the received  $U_{n,[j,k]}$  as follows:

$$\tilde{\mathbf{H}}_n^{\text{up}} = \text{Median}_{1 \leq j \leq Y} \{ \text{sign}_j(d) \cdot U_{n,[j,h_{n,j}(d)]} \}, \quad (21)$$

where  $\text{Median}(\cdot)$  denotes the median of all approximated values. Edge servers aggregate  $\{\tilde{\mathbf{H}}_n^{\text{up}}\}$  directly without decryption, as the orthogonal transformation preserves inner products and norms, ensuring meaningful model averaging. Besides, during the downloading (or distribution) of the hidden layer state, we compress and encrypt it to obtain  $\tilde{\mathbf{H}}_n^{\text{down}}$ .

4) *Communication Modeling*: In ELSA, a symmetric transmission mechanism is employed: intermediate activations are transmitted during the forward pass, while the corresponding gradients are returned during the backward pass. Given that these two components share identical dimensions, the total communication overhead for a single global iteration (e.g.,  $g^{\text{th}}$ ) is

$$C_g = \underbrace{\frac{2\mathbf{t}\zeta\mu D^{\text{hidden}}}{\rho} \sum_{k=1}^K \sum_{n \in \mathbb{N}_k} B_n}_{\text{Client} \leftrightarrow \text{Edge}} + \underbrace{K \cdot |\theta^{\text{LoRA}}|}_{\text{Edge} \rightarrow \text{Cloud}}, \quad (22)$$

where  $\mathbf{t}$  is the number of client–edge collaborative fine-tuning rounds performed within each global aggregation,  $\zeta$  denotes the byte size per floating-point parameter (e.g.,  $\zeta = 4$  for FP32),  $\mu$  represents the input sequence length in tokens, and  $|\theta^{\text{LoRA}}|$  is the total communication volume (in bytes) of the aggregated LoRA adapter parameters uploaded by a single edge server to the cloud. Here,  $B_n$  is the average local mini-batch size used by client  $n$  during training.

The per-client communication latency in the  $g^{\text{th}}$  global round is determined by its local batch size and effective network throughput. Specifically, during  $\mathbf{t}$  rounds of client–edge collaborative training, client  $n$  transmits and receives compressed intermediate activations for  $B_n$  samples per round. Accounting for symmetric forward/backward passes, the total transmitted volume is  $2\mathbf{t}B_n\mu\zeta D^{\text{hidden}}/\rho$ . Dividing by the bandwidth  $\mathcal{B}_n$  of client  $n$ , the communication time is:

$$\mathcal{T}_{g,n} = \frac{2\mathbf{t}B_n\mu\zeta D^{\text{hidden}}/\rho}{\mathcal{B}_n}, \quad (23)$$

Subsequently, the total communication time until convergence is given by

$$T_{\text{total}} \approx G \times \max_{n \in \mathbb{N}_k, k \in \mathcal{K}} (\mathcal{T}_{g,n}), \quad (24)$$

where  $G$  is the number of global iterations required to satisfy the convergence criterion in (16).

### C. Convergence Analysis

**Theorem 1** (Convergence of ELSA). *Under Assumptions 1–3 (in the Appendix A), let the learning rate be  $\eta = \frac{1}{\mathcal{L}\sqrt{G}}$ , where  $G$  is the total number of global iterations. Then, the sequence of global adapter parameters  $\{\theta_g\}_{g=0}^{G-1}$  generated by ELSA satisfies:*

$$\frac{1}{G} \sum_{g=0}^{G-1} \mathbb{E} \left[ \|\nabla \tilde{F}(\theta_g)\|^2 \right] \leq \underbrace{\frac{4\mathcal{L}(\tilde{F}(\theta_0) - \tilde{F}^*)}{\sqrt{G}}}_{\text{optimization error}} + \underbrace{\frac{\sigma_{\text{local}}^2}{\sqrt{G}}}_{\text{vanishing noise}} + \underbrace{\sigma_2^2}_{\text{non-IID bias}},$$

where  $\tilde{F}^* = \min_{\theta} \tilde{F}(\theta)$  denotes the optimal value of the global objective (proof is provided in the Appendix A).

**Remark 1.** *Theorem 1 shows ELSA converges to a neighborhood of a stationary point at rate  $\mathcal{O}(1/\sqrt{G})$ . Although  $\mathcal{O}(1/G)$  non-IID bias reduction is possible under idealized settings (e.g., single-step updates and unbiased aggregation), our multi-round client–edge collaboration, model splitting, and compression introduce a persistent bias between the expected update and the true gradient. This results in a non-vanishing residual error  $\sigma_2^2$ . In contrast, sketching and SGD noise ( $\sigma_{\text{local}}^2$ ) vanish during training. Convergence is ensured by bounding intra-cluster semantic heterogeneity via KLD-based clustering, which aligns local SS-OP bases  $\{U_n\}$  and controls aggregation bias.*

## IV. EXPERIMENTS AND EVALUATIONS

In the following, we aim to evaluate the proposed ELSA framework with respect to two key research questions:

- How does ELSA perform compared to existing methods?
- How do various hyperparameters affect ELSA’s performance, and how can their optimal values be determined?

### A. Experimental Setup

**Datasets:** We consider eight diverse datasets spanning various NLP tasks: (i) *Text Classification (TC)*: *Trec*, *AG\_News*, *Emotion*, and *Banking77*, covering question, news, sentiment, and fine-grained intent classification (up to 77 categories) [40]–[42]; (ii) *Natural Language Inference (NLI)*: *RTE* and *CB*, which involve premise-hypothesis entailment; *MultiRC* and *SQuAD*, representing multi-sentence reading comprehension and extractive question answering tasks respectively [38], [39].

**Baselines:** We evaluate and compare the performance of FedProx [43], FedAMS [44], RaSA [45], FedCada [46], RoFed [19] and FedAvg [47] on the classification task using the test dataset. Additionally, we also study the performance of FedAvg under randomly selected client conditions (i.e., FedAvg(Random)).

**Parameter settings:** Our experimental framework consists of 20 clients and 4 edge servers, deployed within an 8 km  $\times$  8 km area as illustrated in Fig. 2(b). To simulate unreliable client data, we randomly selected 4 clients and injected small batches of mislabeled samples into their local datasets. We adopt BERT-base-uncased as the LLM architecture, which consists of 12 Transformer blocks, a hidden dimension of 768, and 12 attention heads, totaling approximately 110 million parameters [17], [18]. To rigorously evaluate the performance of ELSA,

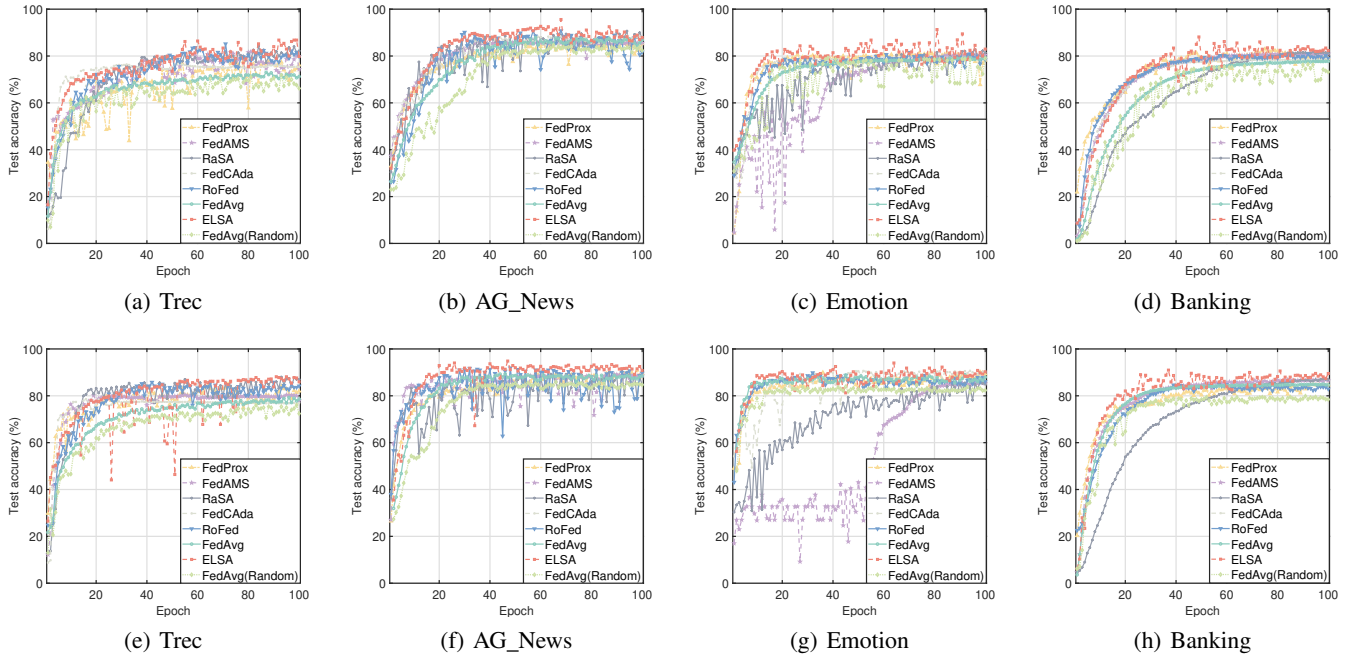


Fig. 4: Test performance comparison across TC datasets under two levels of data heterogeneity: (a)–(d) correspond to  $\hat{\alpha} = 0.1$ , while (e)–(h) use  $\hat{\alpha} = 0.2$ .

TABLE II: Performance comparison on four NLP tasks under different  $\hat{\alpha}$  (0.1 and 0.2). Accuracy (%) is reported for RTE and CB, while F1/EM is reported for MultiRC and SQuAD.

Method	Data Setting $\hat{\alpha} = 0.1$				Data Setting $\hat{\alpha} = 0.2$			
	RTE Accuracy	CB Accuracy	MultiRC F1/EM	SQuAD F1/EM	RTE Accuracy	CB Accuracy	MultiRC F1/EM	SQuAD F1/EM
FedAvg	79.21	80.23	79.61/50.17	76.92/87.06	79.91	81.03	79.96/52.03	77.22/87.72
FedProx	78.92	82.14	80.68/49.19	78.33/87.31	79.54	83.62	81.33/50.02	79.01/87.70
FedAMS	80.13	79.82	81.44/51.33	77.66/86.21	81.22	82.38	81.76/52.05	78.02/87.05
RaSA	78.92	81.24	79.55/51.27	78.38/86.79	80.53	83.24	80.62/52.08	78.99/86.95
FedCAda	79.23	82.66	79.81/51.39	78.52/86.45	81.31	84.23	80.12/52.41	80.03/87.29
RoFed	79.18	82.71	80.22/51.09	78.50/86.55	82.33	83.19	82.19/52.32	79.33/87.16
FedAvg (Random)	78.48	79.26	78.23/48.29	75.33/85.66	79.03	79.77	79.11/49.06	76.52/85.98
<b>ELSA (Ours)</b>	<b>80.93</b>	<b>83.93</b>	<b>81.78/52.06</b>	<b>79.24/87.17</b>	<b>83.13</b>	<b>84.99</b>	<b>82.72/53.16</b>	<b>80.44/88.04</b>
<i>Gain</i>	<i>+0.80</i>	<i>+1.22</i>	<i>+0.34/+0.67</i>	<i>+0.72/-0.14</i>	<i>+0.82</i>	<i>+0.76</i>	<i>+0.63/+0.75</i>	<i>+0.41/+0.32</i>

Note: Values are formatted as ‘performance / improve vs. best baseline’.

we implement a hybrid heterogeneity scheme that simultaneously accounts for quantity skew and label distribution skew: *Quantity Skew*: each client  $n$  allocates a local subset  $\mathcal{D}_n$ , with the size  $|\mathcal{D}_n|$  proportional to a performance factor  $\chi_n = \frac{n+1}{\Omega_k}$ , where  $\Omega_k$  denotes the overall samples related to edge  $k$ ; *Label Distribution Skew*: we impose class imbalance within each local dataset using the Dirichlet distribution  $\text{Dir}(\hat{\alpha})$ . We set  $\hat{\alpha} = \{0.1, 0.2\}$  to simulate varying statistical heterogeneity [48].

### B. Evaluation of Learning Efficiency and Model Performance

To evaluate the model training performance for TC datasets, we prioritize the convergence rate to evaluate the communication efficiency of each method. Conversely, for NLI tasks that demand complex semantic reasoning, we focus on the steady-state performance (e.g., Accuracy, F1 and EM) once training has fully converged. This differentiation ensures that we capture both the learning efficiency on standard tasks

and the ultimate representative capacity on more challenging reasoning benchmarks [18], [19].

As shown in Fig. 4, under the challenging setting of quantity-based heterogeneity, ELSA demonstrates superior convergence behavior across all TC datasets compared to all baselines. Although its initial convergence speed is occasionally slower (e.g., in Fig. 4(a), (d), and (e)), ELSA consistently achieves a higher final accuracy ceiling, indicating better optimization stability. Further, Table II presents the steady-state performance on NLI tasks. ELSA attains state-of-the-art results (e.g., 80.93% on RTE, 81.78% on MultiRC) on all benchmarks except SQuAD, where it is marginally lower than FedProx by only 0.14% in EM. This near-universal superiority, coupled with consistent gains across diverse tasks and heterogeneity levels, highlights ELSA’s strong generalization capability and robustness in practical edge network scenarios.

TABLE III: Comparison of the total communication time to reach target performance across different methods ( $\times 10^3$  s).

Method	AG_News	Banking	Emotion	Trec	RTE	CB	MultiRC	SQuAD
Vanilla Model	10.51	6.01	7.51	3.38	14.41	18.02	39.64	36.93
FedProx	3.65	1.97	2.29	1.04	4.65	5.72	13.73	13.08
FedAMS	3.57	1.89	2.47	1.00	4.58	6.43	14.58	14.16
RaSA	3.43	1.93	2.43	0.98	4.79	6.58	15.73	13.73
FedCAda	3.43	2.32	2.36	0.95	4.72	6.15	14.30	13.30
RoFed	3.36	1.89	2.32	0.97	4.43	6.01	13.44	13.08
FedAvg	3.79	2.14	2.32	1.07	4.58	6.29	14.87	13.94
FedAvg (Random)	3.93	2.22	2.50	1.09	5.00	7.15	16.87	14.58
<b>ELSA (Ours)</b>	<b>3.22/-0.14</b>	<b>1.86/-0.03</b>	<b>2.25/-0.04</b>	<b>0.89/-0.06</b>	<b>4.29/-0.14</b>	<b>5.43/-0.29</b>	<b>13.15/-0.29</b>	<b>12.23/-0.85</b>

Note: Values are formatted as ‘time / reduction vs. best baseline’.

TABLE IV: Sensitivity of ELSA to compression ratio  $\rho$ : performance and communication benefit.

	AG_News	Banking	Emotion	Trec	RTE	CB	MultiRC	SQuAD	Avg. Benefit
	Accuracy	Accuracy	Accuracy	Accuracy	Accuracy	Accuracy	F1/EM	F1/EM	—
$\rho = 2.1$	92.33	86.34	85.22	83.33	84.24	84.18	82.45/53.12	85.66/87.88	—
Comm. Benefit	1.67	1.81	1.66	1.82	1.65	1.26	1.46	1.29	<b>1.58</b>
$\rho = 3.3$	91.08	84.21	85.02	83.08	83.18	84.03	81.87/53.01	84.13/87.48	—
Comm. Benefit	2.98	2.68	2.77	2.68	2.73	2.01	2.45	2.26	<b>2.57</b>
$\rho = 6.4$	86.33	81.03	81.11	81.15	80.25	81.36	81.37/51.71	77.13/86.52	—
Comm. Benefit	3.65	3.84	3.39	4.85	4.46	3.28	3.86	3.12	<b>3.81</b>
$\rho = 8.4$	83.22	75.46	78.22	74.66	75.97	73.66	73.34/47.22	76.22/82.11	—
Comm. Benefit	3.39	4.27	4.33	5.56	3.45	2.24	2.46	3.80	<b>3.69</b>
$\rho = 11.8$	78.03	70.31	72.84	71.81	72.25	68.34	68.19/43.18	72.55/80.06	—
Comm. Benefit	3.98	4.57	4.72	5.82	4.98	5.90	3.77	3.87	<b>4.70</b>

More importantly, the notable performance gap among ELSA, FedAvg, and FedAvg (Random) (e.g., 80.93% vs. 79.21% vs. 78.48% accuracy on RTE under  $\hat{\alpha} = 0.1$ ), highlights the effectiveness of our trust-aware client clustering. ELSA further outperforms all other baselines by explicitly addressing semantic inconsistencies inherent in LLM fine-tuning. Specifically, it rectifies these issues during both client clustering (via behavior-aware semantic fingerprints) and cloud aggregation (via coherence- and trust-weighted fusion), thereby stabilizing local updates and enhancing global model convergence.

### C. Evaluation of Communication Costs and Transmission Efficiency

In the following, we evaluate ELSA by analyzing its communication-utility trade-offs, architectural advantages in model segmentation, and the effectiveness of ‘‘SS-OP + Sketch’’ mechanism in balancing privacy and representation quality, focusing on a setting with  $\hat{\alpha} = 0.1$ ,  $\mathcal{B}_n \in [50, 100]$  Mbps.

#### Analysis of System Utility and Communication Efficiency.

In Fig. 5, we evaluate the practical utility of ELSA by comparing it with an uncompressed Vanilla Model (representing the upper bound of performance without transmission constraints). To achieve comparable performance, the communication volume required by the baseline uncompressed model is  $3.26\times$  to  $3.78\times$  that of ELSA for TC tasks, and up to  $3.64\times$  for NLI tasks. Despite the high compression, ELSA maintains competitive performance, achieving 83.93% accuracy on CB and 81.78% on MultiRC with only marginal degradation compared to the uncompressed upper bound. These results validate that our sketch-based layered compression effectively captures

essential model updates with high fidelity, making it suitable for resource-constrained edge environments.

Furthermore, we extend our evaluation to the total communication time required to reach a predefined convergence target across eight diverse datasets, as summarized in Table III, following (24). Results demonstrate that ELSA consistently achieves the lowest communication latency in all scenarios. Specifically, compared to the uncompressed Vanilla Model, ELSA reduces the total required communication time by approximately 69.3% to 73.7% (e.g., from  $10.51\times 10^3$  s to  $3.22\times 10^3$  s on AG\_News). Even when compared to advanced FL baselines such as FedProx and RaSA, ELSA still yields an average speedup of 6.05% to 12.64%. Notably, on complex tasks such as MultiRC and SQuAD, the reduction in time is most pronounced, highlighting the efficiency of our method in handling complex model updates (e.g., on SQuAD, ELSA further reduces communication time by  $0.85\times 10^3$  compared to RoFed, the fastest method among the baselines).

Next, in Table IV, we present the system performance and communication benefit (it’s measured as the ratio of total communication volume between Vanilla Model and ELSA under identical convergence conditions) of ELSA under different compression strengths  $\rho$  to characterize its sensitivity to compression. We observe that there is a non monotonic relationship between overall communication advantage and compression strength. A lower compression ratio (e.g.  $\rho = 2.1$ ) can ensure high representation fidelity and stable convergence, achieving an accuracy of 92.33% on AG\_News, but the communication burden per training round is significant. While, excessively

TABLE V: Comparison of resource utilization and task completion rate between static and dynamic splitting strategies. Under the original experimental conditions, we further set a heterogeneous network where 40% of clients are resource-constrained. A training task is marked as “Failed” if the iteration latency exceeds the system timeout threshold.

Strategy	Avg. Comp. Util. (%)	Avg. Comm. Util. (%)	Overall Eff. (%)	Task Failure Rate (%)
Static (Aggressive, $p = 1$ )	32.4	<b>88.5</b>	54.2	2.1
Static (Balanced A, $p = 3$ )	45.8	76.3	58.5	8.5
Static (Balanced B, $p = 6$ )	61.2	54.1	56.8	24.3
Static (Conservative, $p = 9$ )	<b>78.5</b>	31.2	48.6	41.7
<b>Ours (Dynamic)</b>	<b>72.3</b>	<b>79.8</b>	<b>84.6</b>	<b>1.2</b>

TABLE VI: Comparison of privacy and utility metrics under different compression rates  $\rho$ .

Method	$\rho = 2.1$			$\rho = 4.2$			$\rho = 8.4$		
	Cos Sim	MSE	Token Acc.	Cos Sim	MSE	Token Acc.	Cos Sim	MSE	Token Acc.
Direct Transmission	1.0000	0.0000	53.13%	–	–	–	–	–	–
Gaussian Noise	0.9137	0.0617	50.11%	–	–	–	–	–	–
Sketch Only	0.3599	2.1509	4.07%	0.2655	4.1584	1.96%	0.1975	7.0615	1.13%
<b>ELSA (<math>r = 8</math>)</b>	<b>-0.0334</b>	<b>2.6979</b>	<b>1.21%</b>	<b>-0.0244</b>	<b>4.7059</b>	<b>0.38%</b>	<b>-0.0220</b>	<b>7.7735</b>	<b>0.09%</b>
<b>ELSA (<math>r = 16</math>)</b>	<b>-0.0167</b>	<b>2.7669</b>	<b>0.45%</b>	<b>-0.0122</b>	<b>4.7046</b>	<b>0.08%</b>	<b>-0.0078</b>	<b>7.7492</b>	<b>0.00%</b>

Note: “–” indicates that the method is independent of the compression ratio  $\rho$  (i.e., no compression is applied).

high compression ratios (e.g.  $\rho = 11.8$ ) can significantly reduce the amount of data transmitted per round, but can lead to a significant decrease in accuracy (e.g. 78.03% on AG\_News). *How to choose the value of  $\rho$ ?* Table IV illustrates the fundamental tradeoff between communication efficiency and model performance induced by the compression ratio  $\rho$ . As  $\rho$  increases, ELSA achieves larger communication benefits (up to a  $4.70 \times$  average reduction at  $\rho = 11.8$ ) but this comes with a noticeable degradation in accuracy and F1/EM across tasks. For small to moderate compression levels ( $\rho = 2.1$  and  $\rho = 3.3$ ), ELSA preserves near-peak performance while already providing meaningful communication savings ( $1.58 \times$ – $2.57 \times$  on average). Beyond this regime, performance drops accelerate, particularly for semantically complex tasks such as MultiRC and SQuAD, indicating that excessive compression increasingly distorts informative hidden representations. Overall, these results suggest that  $\rho \in [2.1, 4.2]$  offers a practical operating region that balances communication efficiency and learning performance, while larger  $\rho$  values should be reserved for severely bandwidth-constrained scenarios.

**Comprehensive Performance Analysis and Ablation Studies.** To rigorously evaluate the effectiveness of ELSA, we conduct a multi-faceted comparison against both SL baselines (e.g., SFLAM [25], SplitLLM [24] and Pri.-Aware SFL [21]) and ablated variants of ELSA. As illustrated in Fig. 6(a), while these baselines offer improvements over the simplified SL, they all exhibit limitations in heterogeneous, non-IID settings. Specifically, SFLAM suffer from resource mismatch, SplitLLM face latency-induced straggler effects, and Pri.-Aware SFL occasionally overfit to local data on complex tasks. In contrast, ELSA across all datasets, achieving an average accuracy gain of 0.62% over the second-best method (although we are slightly lower than Pri.-Aware SFL on AG\_News). This demonstrates the superior robustness of our integrated design in handling device heterogeneity and data distribution shifts. Further, to

isolate the contribution of our core modules, we perform ablation studies against two specific variants of ELSA: (i) *ELSA-Fixed*: Our framework with the *dynamic splitting strategy disabled*, reverting to a static partition ( $p = 6, q = 4, o = 2$ ); (ii) *ELSA-NoCluster*: Our framework with the *behavior-aware KLD clustering disabled*, relying instead on random or distance-based client assignment. The results reveal critical insights. ELSA significantly outperforms both ELSA-Fixed and ELSA-NoCluster, which confirms that our *resource-aware dynamic splitting* is essential for adapting to diverse hardware capabilities without incurring timeouts, while our *KLD-based behavioral profiling* effectively mitigates non-IID data heterogeneity by grouping semantically similar clients. In summary, ELSA’s superiority over both external baselines and internal ablated variants confirms that the synergy between *adaptive model splitting* and *behavior-aware hierarchical aggregation* is key to achieving high-performance, efficient, and robust distributed LLM fine-tuning.

**Impact of Model Segmentation.** We evaluate the performance of ELSA by varying the number of transformer blocks trained locally on the client side, specifically, we evaluate  $p \in \{1, 3, 6, 9\}$ , with corresponding  $(q, o)$  pairs of  $(9, 2)$ ,  $(7, 2)$ ,  $(4, 2)$  and  $(1, 2)$ <sup>1</sup>, respectively, ensuring the total number of transformer blocks remains 12. As illustrated in the radar chart in Fig. 6(b), a significant performance degradation is observed as the number of local blocks increases to 6. We attribute this phenomenon to a critical factors inherent in SL paradigms. Although our hierarchical aggregation mechanism, to some extent, can avoid local optima of the model at the client end, upon having large number of training layers, it still has a certain impact, that is, the feature extractor becomes “too personalized” to the local (usually non-IID) data distribution and cannot capture a universal semantic representation. Furthermore, these

<sup>1</sup>In our experiments,  $o$  was empirically set to 2, but it has no bearing on the overall findings since our analysis focuses on the relative changes in  $p$ .

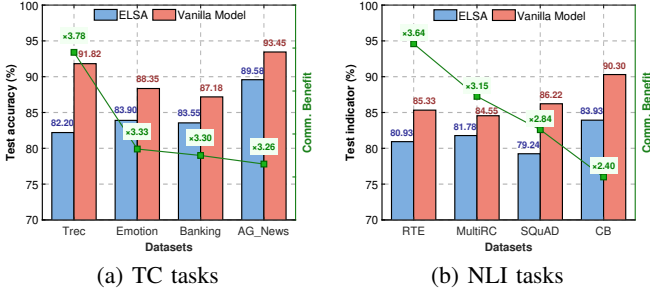


Fig. 5: Evaluation performance and communication reduction of ELSA versus uncompressed schemes on various datasets (Indicator are Accuracy (RTE, CB) and F1 (MultiRC, SQuAD), compression ratio  $\rho = 4.2$ ).

findings suggest that maintaining a client-side training depth of fewer than 6 Transformer blocks is sufficient to yield robust results. Building on this insight, we configure our *resource-aware dynamic splitting* strategy with an upper bound  $p_{\max} = 6$  to prevent performance degradation from over-personalization, while allowing  $p_n$  to adaptively decrease for clients with better resources.

Table V illustrates the performance trade-offs between fixed splitting configurations and our proposed dynamic strategy in a heterogeneous environment. Static strategies face a dilemma: aggressive offloading (e.g.,  $p = 1$ ) leads to high communication overhead, causing a notable task failure rate for bandwidth-constrained clients. Conversely, conservative local training (e.g.,  $p = 9$ ) ensures task completion but results in poor overall efficiency (48.6%) as computationally weak clients become stragglers. In contrast, our *resource-aware dynamic splitting* adaptively assigns  $p_n$  based on each client’s specific computational and network profile. This approach achieves the highest overall efficiency (84.6%) while maintaining the lowest failure rate (1.2%), demonstrating its ability to effectively balance system efficiency and robustness against device heterogeneity<sup>2</sup>. As observed in Fig. 6(b), while the static configuration with minimal local layers ( $p = 1$ ) achieves the marginal highest accuracy in ideal conditions, it incurs prohibitive communication costs and high failure rates as discussed in Table V. In contrast, our dynamic approach surpasses both the  $p = 3$  and  $p = 6$  static baselines on average, while significantly outperforming the conservative  $p = 9$  setting. Specifically, our method closely tracks the performance of the  $p = 3$  configuration on most datasets (e.g., SQuAD, MultiRC, CB) while occasionally approaching the  $p = 1$  peak on others (e.g., AG\_News and Emotion). This demonstrates that by capping the local depth at the empirically determined threshold ( $p_{\max} = 6$ ) and dynamically offloading the rest, ELSA successfully navigates the trade-off: it retains the generalization benefits of shallow local training (avoiding the  $p = 9$  drop) while accommodating

<sup>2</sup>Comp. Util. denotes the average percentage of client computational capacity (FLOPS) actively engaged in training; Comm. Util. represents the average fraction of available network bandwidth effectively used for data transmission; Overall Eff. is a composite score evaluating the joint efficiency of computation and communication resources; Task Failure Rate indicates the proportion of clients unable to complete an iteration within the system timeout limit, reflecting robustness against stragglers.

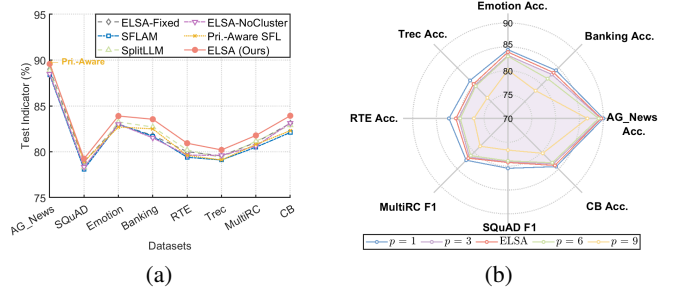


Fig. 6: Left subplot: ELSA vs. Existing baselines and Ablated variants: a performance comparison; Right subplot: effects of collaborative training schemes on model performance.

heterogeneous resource constraints without the instability of aggressive static offloading ( $p = 1$ ).

**Quantitative Analysis of Data Desensitization and Privacy.** Table VI evaluates the trade-off between privacy and utility in our SS-OP + Sketch under varying compression ratios. To simulate potential attacks on intermediate activations during client–edge transmissions, we adopt two threat models following [49], [50]: (i) Reconstruction attacks by a semi-honest server, measured via cosine similarity (Cos Sim) and mean squared error (MSE) between original and reconstructed hidden states; (ii) Token identification attacks, where an adversary attempts to infer input tokens from compressed representations, evaluated by token recovery accuracy (Token Acc.). We compare against three baselines: (i) Direct Transmission (no protection), (ii) Gaussian Noise (adding calibrated noise for differential privacy  $\mathcal{N}(0, 0.25)$ ), and (iii) Sketch Only (compression without orthogonal perturbation).

As shown in Table VI, Direct Transmission is highly vulnerable (Cos Sim = 1.0, Token Acc. = 53.13%), while Gaussian Noise offers only marginal protection (Cos Sim = 0.9137). Sketch Only reduces token recovery (e.g., 1.13% at  $\rho = 8.4$ ) but retains exploitable semantic structure, as indicated by its positive cosine similarity. In contrast, ELSA integrates SS-OP with sketching, driving cosine similarity to near or below zero and suppressing token accuracy to near-zero levels. Notably, increasing the semantic subspace dimension from  $r = 8$  to  $r = 16$  further reduces token identification accuracy (e.g., from 0.38% to 0.08% at  $\rho = 4.2$ ) while maintaining similarly low cosine similarity. This suggests that, under appropriate compression ratios, a larger  $r$  enhances privacy by perturbing a richer set of semantic directions without degrading utility. The slight MSE increase over Sketch Only is benign for training, confirming that ELSA<sup>3</sup> achieves strong privacy without sacrificing utility.

## V. CONCLUSION

We proposed ELSA, a privacy-aware and efficient HFL framework designed to optimize distributed LLM fine-tuning in heterogeneous and resource-constrained edge environments. By synergistically integrating SL with a hierarchical architecture,

<sup>3</sup>Note that while these modules introduce additional operations, their computational cost is designed to be lightweight relative to the LLM forward/backward pass (see Appendix B for detailed complexity analysis).

ELSA addresses the coupled challenges of computational fragmentation, data heterogeneity, and communication overhead. Extensive evaluations across eight diverse NLP benchmarks, demonstrated that ELSA consistently outperforms state-of-the-art baselines in both learning efficiency and final performance. Future research directions include the extension of ELSA to ultra-large-scale models with substantially increased parameter counts, such as LLaMA- and GPT-scale architectures. In addition, joint intelligent mechanisms for model segmentation and communication compression can be explored to enable dynamic optimization of split depth and compression ratios in response to more severe real-time edge resource availability and network dynamics.

## REFERENCES

- [1] H. Luo, Y. Liu, R. Zhang, J. Wang, G. Sun, and D. Niyato, "Toward Edge General Intelligence with Multiple-Large Language Model (Multi-LLM): Architecture, Trust, and Orchestration," *IEEE Trans. Cogn. Commun. Netw.*, vol. 11, no. 6, pp. 3563–3585, 2025.
- [2] M. Zhang, X. Shen, J. Cao, Z. Cui, and S. Jiang, "EdgeShard: Efficient LLM Inference via Collaborative Edge Computing," *IEEE Internet Things J.*, vol. 12, no. 10, pp. 13119–13131, 2025.
- [3] C. Liu and J. Zhao, "Enhancing Stability and Resource Efficiency in LLM Training for Edge-Assisted Mobile Systems," *IEEE Trans. Mobile Comput.*, vol. 25, no. 1, pp. 1–18, 2026.
- [4] D. Farr, N. Manzonelli, I. Cruickshank, and J. West, "RED-CT: A systems design methodology for using LLM-labeled data to train and deploy edge linguistic classifiers," in *COLING*, pp. 58–67, 2025.
- [5] J. Yang, Q. Wu, Z. Feng, Z. Zhou, D. Guo, and X. Chen, "Quality-of-Service Aware LLM Routing for Edge Computing With Multiple Experts," *IEEE Trans. Mobile Comput.*, vol. 24, no. 12, pp. 13648–13662, 2025.
- [6] H. Liu, D. Tam, M. Muqeeth, J. Mohta, T. Huang, M. Bansal, *et al.*, "Few-Shot Parameter-Efficient Fine-Tuning is Better and Cheaper than In-Context Learning," in *NeurIPS*, vol. 35, pp. 1950–1965, 2022.
- [7] L. Xu, H. Xie, S.-Z. J. Qin, X. Tao, and F. L. Wang, "Parameter-Efficient Fine-Tuning Methods for Pretrained Language Models: A Critical Review and Assessment," *arXiv preprint arXiv:2312.12148*, 2023.
- [8] Z. Mai, A. Chowdhury, P. Zhang, C.-H. Tu, H.-Y. Chen, V. Pahuja, *et al.*, "Fine-Tuning is Fine, if Calibrated," in *NeurIPS*, vol. 37, pp. 136084–136119, 2024.
- [9] W. Yang, X. Hu, X. Zhu, R. Wu, W. Pedrycz, X. Liu, *et al.*, "FedMPS: Federated Learning in a Synergy of Multi-Level Prototype-Based Contrastive Learning and Soft Label Generation," *IEEE Trans. Neural Netw. Learn. Syst.*, pp. 1–1, 2025.
- [10] H. Chen, X. Xu, X. Zhu, X. Zhou, F. Dai, Y. Gao, *et al.*, "Where Does This Data Come From? Enhanced Source Inference Attacks in Federated Learning," in *IJCAI*, pp. 4815–4823, 2025.
- [11] X. Chen, G. Xu, X. Xu, H. Jiang, Z. Tian, and T. Ma, "Multicenter Hierarchical Federated Learning With Fault-Tolerance Mechanisms for Resilient Edge Computing Networks," *IEEE Trans. Neural Netw. Learn. Syst.*, vol. 36, no. 1, pp. 47–61, 2025.
- [12] J. Lu, Y. Chen, S. Cao, L. Chen, W. Wang, and Y. Xin, "LEAP: Optimization Hierarchical Federated Learning on Non-IID Data with Coalition Formation Game," in *IJCAI*, pp. 4660–4668, 2024.
- [13] B. Wu, F. Fang, X. Wang, D. Cai, S. Fu, and Z. Ding, "Client Selection and Cost-Efficient Joint Optimization for NOMA-Enabled Hierarchical Federated Learning," *IEEE Trans. Wireless Commun.*, vol. 23, no. 10, pp. 14289–14303, 2024.
- [14] Z. Lin, G. Zhu, Y. Deng, X. Chen, Y. Gao, K. Huang, *et al.*, "Efficient Parallel Split Learning over Resource-Constrained Wireless Edge Networks," *IEEE Trans. Mobile Comput.*, vol. 23, no. 10, pp. 9224–9239, 2024.
- [15] B.-H. Kim, A. Haldorai, and S. Suprakash, "A Battery Lifetime Monitoring and Estimation Using Split Learning Algorithm in Smart Mobile Consumer Electronics," *IEEE Trans. Consum. Electron.*, vol. 70, no. 3, pp. 5942–5951, 2024.
- [16] W. Liang, X. Chen, S. Huang, G. Xiong, K. Yan, and X. Zhou, "Federal Learning Edge Network Based Sentiment Analysis Combating Global COVID-19," *Computer Communications*, vol. 204, pp. 33–42, 2023.
- [17] Y. Tian, Y. Wan, L. Lyu, D. Yao, H. Jin, and L. Sun, "FedBERT: When Federated Learning Meets Pre-training," *ACM Trans. Intell. Syst. Technol.*, vol. 13, no. 4, 2022.
- [18] J. Tang, Z. Huang, and C. Li, "MT-FBERT: Malicious Traffic Detection Based on Efficient Federated Learning of BERT," *Future Internet*, vol. 17, no. 8, 2025.
- [19] H. Wang, Z. Yin, B. Chen, Y. Zeng, X. Yan, C. Zhou, *et al.*, "ROFED-LLM: Robust Federated Learning for Large Language Models in Adversarial Wireless Environments," *IEEE Trans. Netw. Sci. Eng.*, pp. 1084–1096, 2026.
- [20] K. Yang, R. Li, and Y. Xu, "LLM Enabled Resource Allocation for Knowledge Base Federated-Split Learning in Semantic Communications," *IEEE Trans. Consum. Electron.*, pp. 1–1, 2026.
- [21] X. Chen, W. Wu, F. Ji, Y. Lu, and L. Li, "Privacy-Aware Split Federated Learning for LLM Fine-Tuning Over Internet of Things," *IEEE Internet Things J.*, vol. 12, no. 24, pp. 51902–51913, 2025.
- [22] Z. Lin, X. Hu, Y. Zhang, Z. Chen, Z. Fang, X. Chen, A. Li, P. Vepakomma, and Y. Gao, "Splitlora: A split parameter-efficient fine-tuning framework for large language models," *arXiv preprint arXiv:2407.00952*, 2024.
- [23] J. Ma, X. Lyu, J. Jiang, Q. Cui, H. Yao, and X. Tao, "Split-Frozen: Split Learning with Device-side Model Frozen for Fine-Tuning LLM on Heterogeneous Resource-Constrained Devices," *arXiv preprint arXiv:2503.18986*, 2025.
- [24] S. Zhang, G. Cheng, Z. Li, and W. Wu, "SplitLLM: Hierarchical Split Learning for Large Language Model over Wireless Network," in *IEEE Globecom Workshops (GC Wkshps)*, pp. 1–6, 2024.
- [25] X. Qiang, H. Liu, X. Zhang, Z. Chang, and Y.-C. Liang, "Deploying Large AI Models on Resource-Limited Devices with Split Federated Learning," *arXiv preprint arXiv:2504.09114*, 2025.
- [26] S. Zhang, G. Cheng, W. Wu, X. Huang, L. Song, and X. Shen, "Split Fine-Tuning for Large Language Models in Wireless Networks," *IEEE J. Sel. Topics Signal Process.*, vol. 19, no. 7, pp. 1376–1391, 2025.
- [27] Z. Wang, G. Yang, H. Dai, and C. Rong, "Privacy-Preserving Split Learning for Large-Scaled Vision Pre-Training," *IEEE Trans. Inf. Forensics Security*, vol. 18, pp. 1539–1553, 2023.
- [28] D. Qiao, X. Ao, Y. Liu, X. Chen, F. Song, Z. Qin, *et al.*, "Tri-AFLLM: Resource-Efficient Adaptive Asynchronous Accelerated Federated LLMs," *IEEE Trans. Circuits Syst. Video Technol.*, vol. 35, no. 5, pp. 4198–4211, 2025.
- [29] S. Ding and C. Hu, "eFedLLM: Efficient LLM Inference Based on Federated Learning," *arXiv preprint arXiv:2411.16003*, 2024.
- [30] C. Zhang, G. Shan, B.-h. Roh, and J. Jiang, "FM2 Learning: LLM-Based Federated Multi-Task Multi-Domain Learning for Consumer Electronics and IoT Enhancement," *IEEE Trans. Consum. Electron.*, pp. 1–1, 2025.
- [31] J. Chen, S. Guo, Q. Qi, J. Hao, S. Guo, and X. Qiu, "Enabling Foundation Models: A Distributed Collaboration Framework Based on Graph Federated Learning," *IEEE Trans. Serv. Comput.*, vol. 17, no. 6, pp. 3569–3582, 2024.
- [32] W. Fang, D.-J. Han, E. Chen, S. Wang, and C. G. Brinton, "Hierarchical Federated Learning with Multi-Timescale Gradient Correction," in *NeurIPS*, pp. 78863–78904, 2024.
- [33] Y. Sai, X. Wu, J. Jiang, Y. Huang, Q. Yan, Z. Li, *et al.*, "Optimizing Hierarchical Federated Learning: A Reinforcement Learning Approach," *IEEE Trans. Consum. Electron.*, vol. 71, no. 2, pp. 4076–4086, 2025.
- [34] J. Tian and Y. Yuan, "HFL-FlowLLM: Large Language Models for Network Traffic Flow Classification in Heterogeneous Federated Learning," *arXiv preprint arXiv:2511.14199*, 2025.
- [35] Z. Cheng, X. Xia, M. Liwang, X. Fan, Y. Sun, X. Wang, *et al.*, "CHEESE: Distributed Clustering-Based Hybrid Federated Split Learning Over Edge Networks," *IEEE Trans. Parallel Distrib. Syst.*, vol. 34, no. 12, pp. 3174–3191, 2023.
- [36] M. Rahad, R. Shabab, M. S. Ahammad, M. M. Reza, A. Karmaker, and M. A. Hossain, "KL-FedDis: A Federated Learning Approach with Distribution Information Sharing using Kullback-Leibler Divergence for non-IID Data," *Neuroscience Informatics*, vol. 5, no. 1, p. 100182, 2025.
- [37] X. Yang, M. Liwang, L. Fu, Y. Su, S. Hosseinalipour, X. Wang, and Y. Hong, "Adaptive UAV-Assisted Hierarchical Federated Learning: Optimizing Energy, Latency, and Resilience for Dynamic Smart IoT," *IEEE Trans. Serv. Comput.*, vol. 18, no. 6, pp. 3420–3434, 2025.
- [38] A. Wang, Y. Pruksachatkun, N. Nangia, A. Singh, J. Michael, F. Hill, O. Levy, and S. R. Bowman, "SuperGLUE: A Stickier Benchmark for General-purpose Language Understanding Systems," in *NeurIPS*, pp. 3266 – 3280, 2019.

- [39] P. Rajpurkar, J. Zhang, K. Lopyrev, and P. Liang, “SQuAD: 100,000+ Questions for Machine Comprehension of Text,” in *NeurIPS*, pp. 2383–2392, 2016.
- [40] X. Li and D. Roth, “Learning Question Classifiers,” in *COLING*, 2002.
- [41] X. Zhang, J. Zhao, and Y. LeCun, “Character-Level Convolutional Networks for Text Classification,” in *NeurIPS*, p. 649–657, 2015.
- [42] O. Oluwatobi and T. M. Erik, “DLGNet: A Transformer-Based Model for Dialogue Response Generation,” in *Workshop NLP for Conversational AI*, pp. 54–62, 2020.
- [43] T. Li, A. K. Sahu, M. Zaheer, M. Sanjabi, A. Talwalkar, and V. Smith, “Federated Optimization in Heterogeneous Networks,” in *MLSys*, vol. 2, pp. 429–450, 2020.
- [44] Y. Wang, L. Lin, and J. Chen, “Communication-Efficient Adaptive Federated Learning,” in *ICML*, pp. 22802–22838, 2022.
- [45] L. Wang, M. Huang, Z. Zhang, M. Li, J. Wang, and K. Gai, “RaSA: Robust and Adaptive Secure Aggregation for Edge-Assisted Hierarchical Federated Learning,” *IEEE Trans. Inf. Forensics Security*, vol. 20, pp. 4280–4295, 2025.
- [46] L. Zhou, Y. He, K. Zhai, X. Liu, S. Liu, X. Ma, *et al.*, “FedCAda: Adaptive Client-Side Optimization for Accelerated and Stable Federated Learning,” in *ICASSP*, pp. 1–5, 2025.
- [47] B. McMahan, E. Moore, D. Ramage, S. Hampson, and B. A. y. Arcas, “Communication-Efficient Learning of Deep Networks from Decentralized Data,” in *AISTATS*, vol. 54, pp. 1273–1282, 2017.
- [48] L. Gao, H. Fu, L. Li, Y. Chen, M. Xu, and C.-Z. Xu, “FedDC: Federated Learning with Non-IID Data via Local Drift Decoupling and Correction,” in *CVPR*, pp. 10102–10111, 2022.
- [49] H. Li, M. Xu, and Y. Song, “Sentence Embedding Leaks More Information than You Expect: Generative Embedding Inversion Attack to Recover the Whole Sentence,” in *Findings of ACL*, pp. 14022–14040, 2023.
- [50] Z. Wan, A. Cheng, Y. Wang, and L. Wang, “Information leakage from embedding in large language models,” *arXiv preprint arXiv:2405.11916*, 2024.
- [51] Q. Chen, Z. Wang, M. Yan, H. Yan, X. Lin, and J. Zhou, “DeFedGCN: Privacy-Preserving Decentralized Federated GCN for Recommender System,” *IEEE Trans. Serv. Comput.*, vol. 18, no. 2, pp. 729–742, 2025.
- [52] F. Haddadpour, B. Karimi, P. Li, and X. Li, “FedSKETCH: Communication-Efficient and Private Federated Learning via Sketching,” *arXiv preprint arXiv:2008.04975*, 2020.

## A. Proof of Theorem 1

To analyze the convergence of ELSA, we first note that only the adapter parameters  $\theta$  are trainable, while the pre-trained LLM backbone remains frozen throughout fine-tuning and is thus omitted from the optimization arguments. We then establish convergence under the following standard assumptions [51]:

**Assumption 1** (Lipschitz Smoothness of Local Loss Functions). *There exists  $\mathcal{L} > 0$  such that for each client  $n$  and any parameter vectors  $\theta, \theta'$ ,*

$$\|\nabla F_n(\theta) - \nabla F_n(\theta')\| \leq \mathcal{L} \|\theta - \theta'\|, \quad \forall n, \theta, \theta'. \quad (25)$$

**Assumption 2** (Bounded SGD Variance and non-IID Heterogeneity). *There exist constants  $\sigma_1^2, \sigma_2^2 > 0$  such that*

$$\mathbb{E} \left[ \|\nabla F_n(\theta) - \nabla f_n(\theta; \mathbf{b})\|^2 \right] \leq \sigma_1^2, \quad (\text{Local SGD variance}) \quad (26)$$

$$\left\| \nabla F_n(\theta) - \nabla \tilde{F}(\theta) \right\|^2 \leq \sigma_2^2, \quad (\text{non-IID data heterogeneity}) \quad (27)$$

where  $f_n(\cdot; \mathbf{b})$  denotes the loss on a mini-batch  $\mathbf{b}$  sampled from client  $n$ 's local data, and  $\tilde{F}(\theta) = \frac{1}{N} \sum_{n=1}^N F_n(\theta)$  is the global objective.

**Assumption 3** (Error from Sketching and Median Reconstruction). *The SS-OP transformation is orthogonal and preserves norms and inner products without bias. However, the subsequent hash-based sketching and median-based reconstruction introduce approximation errors. Specifically, the reconstructed hidden state  $\tilde{\mathbf{H}}_n^{\text{up}}$  satisfies:*

$$\left\| \mathbb{E}[\tilde{\mathbf{H}}_n^{\text{up}}] - \mathbf{H}_n^{\text{up}} \right\| \leq \epsilon_{\text{sketch}}, \quad (\text{Bias}) \quad (28)$$

$$\mathbb{E} \left[ \left\| \tilde{\mathbf{H}}_n^{\text{up}} - \mathbb{E}[\tilde{\mathbf{H}}_n^{\text{up}}] \right\|^2 \right] \leq \sigma_{\text{sketch}}^2, \quad (\text{Variance}) \quad (29)$$

where  $\epsilon_{\text{sketch}}$  arises from the bias of the median estimator, and  $\sigma_{\text{sketch}}^2$  accounts for variance due to hashing collisions. The total mean squared error is bounded by  $\delta^2 \triangleq \epsilon_{\text{sketch}}^2 + \sigma_{\text{sketch}}^2$ .

Under Assumption 1, the reconstruction error in hidden states induces a bounded error in the computed gradients. Extending Lemma 1 of [52] to the biased setting, the gradient  $\mathbf{g}_n$  computed using the reconstructed states satisfies:

$$\mathbb{E} \left[ \|\mathbf{g}_n - \nabla F_n(\theta)\|^2 \right] \leq \underbrace{\mathbb{E} \left[ \|\nabla f_n(\theta; \mathbf{b}) - \nabla F_n(\theta)\|^2 \right]}_{\leq \sigma_1^2} + \underbrace{\mathcal{L}^2 \delta^2}_{\text{sketching error}} \triangleq \sigma_{\text{local}}^2. \quad (30)$$

Here,  $\sigma_{\text{local}}^2$  captures the combined effect of stochastic sampling and sketching-induced noise at each client.

Critically, the non-IID data heterogeneity (Assumption 2) is not absorbed into  $\sigma_{\text{local}}^2$ ; instead, it manifests as a systematic deviation between local and global gradients. Let  $\mathbf{r}_g$  denote the aggregated update direction after client-side computation,

compression, and server-side averaging. Then, the total error relative to the true global gradient satisfies:

$$\mathbb{E} \left[ \left\| \mathbf{r}_g - \nabla \tilde{F}(\theta_g) \right\|^2 \right] \leq \frac{1}{N} \sum_{n=1}^N \mathbb{E} \left[ \|\mathbf{g}_n - \nabla F_n(\theta_g)\|^2 \right] + \frac{1}{N} \sum_{n=1}^N \left\| \nabla F_n(\theta_g) - \nabla \tilde{F}(\theta_g) \right\|^2 \leq \sigma_{\text{local}}^2 + \sigma_2^2. \quad (31)$$

This decomposition explicitly separates the impact of *local randomness* ( $\sigma_{\text{local}}^2$ ) from *data heterogeneity* ( $\sigma_2^2$ ), ensuring a theoretically sound convergence characterization.

Building upon the above error decomposition, we establish the following convergence guarantee for ELSA.

*Proof.* By Assumption 1 (Lipschitz smoothness of  $\tilde{F}(\cdot)$ ), the following inequality holds for any global iteration  $g$ :

$$\tilde{F}(\theta_{g+1}) \leq \tilde{F}(\theta_g) - \eta \langle \nabla \tilde{F}(\theta_g), \mathbf{r}_g \rangle + \frac{\mathcal{L}\eta^2}{2} \|\mathbf{r}_g\|^2. \quad (32)$$

Taking expectation over the randomness in SGD and sketching, we decompose the update direction as:

$$\mathbb{E}[\mathbf{r}_g] = \nabla \tilde{F}(\theta_g) + \underbrace{\left( \mathbb{E}[\mathbf{r}_g] - \nabla \tilde{F}(\theta_g) \right)}_{\text{zero-mean under unbiased aggregation}}, \quad (33)$$

but more importantly, from the error decomposition in Section III.C, we have:

$$\mathbb{E} \left[ \left\| \mathbf{r}_g - \nabla \tilde{F}(\theta_g) \right\|^2 \right] \leq \sigma_{\text{local}}^2 + \sigma_2^2. \quad (34)$$

We now bound the two key terms in the smoothness inequality.

**(Step 1) Inner product term.** Using the identity  $\mathbb{E}[\langle a, X \rangle] = \langle a, \mathbb{E}[X] \rangle$ , we get:

$$\begin{aligned} -\mathbb{E}[\langle \nabla \tilde{F}(\theta_g), \mathbf{r}_g \rangle] &= -\langle \nabla \tilde{F}(\theta_g), \mathbb{E}[\mathbf{r}_g] \rangle \\ &= -\|\nabla \tilde{F}(\theta_g)\|^2 - \langle \nabla \tilde{F}(\theta_g), \mathbb{E}[\mathbf{r}_g] - \nabla \tilde{F}(\theta_g) \rangle. \end{aligned} \quad (35)$$

Applying Cauchy-Schwarz and Young's inequality ( $ab \leq \frac{a^2}{2} + \frac{b^2}{2}$ ):

$$\begin{aligned} -\langle \nabla \tilde{F}(\theta_g), \mathbb{E}[\mathbf{r}_g] - \nabla \tilde{F}(\theta_g) \rangle &\leq \|\nabla \tilde{F}(\theta_g)\| \cdot \|\mathbb{E}[\mathbf{r}_g] - \nabla \tilde{F}(\theta_g)\| \\ &\leq \frac{1}{2} \|\nabla \tilde{F}(\theta_g)\|^2 + \frac{1}{2} \|\mathbb{E}[\mathbf{r}_g] - \nabla \tilde{F}(\theta_g)\|^2. \end{aligned} \quad (36)$$

Note that by Jensen's inequality,

$$\|\mathbb{E}[\mathbf{r}_g] - \nabla \tilde{F}(\theta_g)\|^2 \leq \mathbb{E}[\|\mathbf{r}_g - \nabla \tilde{F}(\theta_g)\|^2] \leq \sigma_{\text{local}}^2 + \sigma_2^2.$$

Thus,

$$-\mathbb{E}[\langle \nabla \tilde{F}(\theta_g), \mathbf{r}_g \rangle] \leq -\frac{1}{2} \|\nabla \tilde{F}(\theta_g)\|^2 + \frac{1}{2} (\sigma_{\text{local}}^2 + \sigma_2^2). \quad (37)$$

**(Step 2) Quadratic term.** Using  $\|a + b\|^2 \leq 2\|a\|^2 + 2\|b\|^2$ ,

$$\begin{aligned} \mathbb{E}[\|\mathbf{r}_g\|^2] &= \mathbb{E}[\|\mathbf{r}_g - \nabla \tilde{F}(\theta_g) + \nabla \tilde{F}(\theta_g)\|^2] \\ &\leq 2\mathbb{E}[\|\mathbf{r}_g - \nabla \tilde{F}(\theta_g)\|^2] + 2\|\nabla \tilde{F}(\theta_g)\|^2 \\ &\leq 2(\sigma_{\text{local}}^2 + \sigma_2^2) + 2\|\nabla \tilde{F}(\theta_g)\|^2. \end{aligned} \quad (38)$$

Substituting (Step 1) and (Step 2) into the smoothness inequality:

$$\begin{aligned}\mathbb{E}[\tilde{F}(\theta_{g+1})] &\leq \tilde{F}(\theta_g) - \eta \left( \frac{1}{2} \|\nabla \tilde{F}(\theta_g)\|^2 - \frac{1}{2} (\sigma_{\text{local}}^2 + \sigma_2^2) \right) \\ &\quad + \frac{\mathcal{L}\eta^2}{2} \left( 2(\sigma_{\text{local}}^2 + \sigma_2^2) + 2\|\nabla \tilde{F}(\theta_g)\|^2 \right) \\ &= \tilde{F}(\theta_g) - \left( \frac{\eta}{2} - \mathcal{L}\eta^2 \right) \|\nabla \tilde{F}(\theta_g)\|^2 \\ &\quad + \frac{\eta}{2} (\sigma_{\text{local}}^2 + \sigma_2^2) + \mathcal{L}\eta^2 (\sigma_{\text{local}}^2 + \sigma_2^2).\end{aligned}\quad (39)$$

Choose learning rate  $\eta = \frac{1}{\mathcal{L}\sqrt{G}}$ . For  $G \geq 4$ , we have  $\mathcal{L}\eta \leq \frac{1}{2}$ , so  $\frac{\eta}{2} - \mathcal{L}\eta^2 \geq \frac{\eta}{4}$ . Rearranging:

$$\frac{\eta}{4} \|\nabla \tilde{F}(\theta_g)\|^2 \leq \tilde{F}(\theta_g) - \mathbb{E}[\tilde{F}(\theta_{g+1})] + \left( \frac{\eta}{2} + \mathcal{L}\eta^2 \right) (\sigma_{\text{local}}^2 + \sigma_2^2).\quad (40)$$

Summing over  $g = 0$  to  $G - 1$  and taking total expectation:

$$\begin{aligned}\frac{\eta}{4} \sum_{g=0}^{G-1} \mathbb{E}[\|\nabla \tilde{F}(\theta_g)\|^2] &\leq \tilde{F}(\theta_0) - \tilde{F}(\theta_G) + G \left( \frac{\eta}{2} + \mathcal{L}\eta^2 \right) (\sigma_{\text{local}}^2 + \sigma_2^2) \\ &\leq \tilde{F}(\theta_0) - \tilde{F}^* + G \left( \frac{\eta}{2} + \mathcal{L}\eta^2 \right) (\sigma_{\text{local}}^2 + \sigma_2^2).\end{aligned}\quad (41)$$

where  $\tilde{F}^* = \min_{\theta} \tilde{F}(\theta)$ . Then, dividing both sides by  $\frac{\eta}{4}G$ :

$$\begin{aligned}\frac{1}{G} \sum_{g=0}^{G-1} \mathbb{E}[\|\nabla \tilde{F}(\theta_g)\|^2] &\leq \frac{4(\tilde{F}(\theta_0) - \tilde{F}^*)}{\eta G} + \\ &\quad 4 \left( \frac{1}{2} + \mathcal{L}\eta \right) (\sigma_{\text{local}}^2 + \sigma_2^2) \\ &= \frac{4\mathcal{L}(\tilde{F}(\theta_0) - \tilde{F}^*)}{\sqrt{G}} + 4 \left( \frac{1}{2} + \frac{1}{\sqrt{G}} \right) (\sigma_{\text{local}}^2 + \sigma_2^2).\end{aligned}\quad (42)$$

For sufficiently large  $G$  (e.g.,  $G \geq 4$ ),  $\frac{1}{\sqrt{G}} \leq \frac{1}{2}$ , so  $\frac{1}{2} + \frac{1}{\sqrt{G}} \leq 1$ . Thus,

$$\frac{1}{G} \sum_{g=0}^{G-1} \mathbb{E}[\|\nabla \tilde{F}(\theta_g)\|^2] \leq \frac{4\mathcal{L}(\tilde{F}(\theta_0) - \tilde{F}^*)}{\sqrt{G}} + \frac{\sigma_{\text{local}}^2}{\sqrt{G}} + \sigma_2^2,\quad (43)$$

where we absorb constants into the  $\frac{\sigma_{\text{local}}^2}{\sqrt{G}}$  term for clarity (since  $\sigma_{\text{local}}^2$  already includes problem-dependent constants). This matches the bound in Theorem 1, completing the proof.  $\square$

## B. Computational Overhead Analysis

**Remark 2** (Computational Overhead in Resource-Constrained Settings). *A natural concern regarding ELSA is whether the additional modules—behavioral probing, SS-OP, and sketch-based compression, introduce prohibitive computational overhead on resource-constrained edge devices. We address this concern through three complementary analyses:*

### (i) Module-wise Complexity Characterization.

- **Behavioral Probing:** The construction of Gaussian behavioral fingerprints (Step 1–2, Section III.B.1) requires a single forward pass of  $Q$  public probe samples ( $Q \ll \|\mathcal{D}_n\|$ ) to extract [CLS] embeddings. This operation is performed **only during the initialization phase** (or infrequently upon significant data drift), yielding an amortized cost

of  $\mathcal{O}(Q \cdot D_{\text{hidden}})$  per client, which is negligible compared to full-dataset fine-tuning.

- **SS-OP:** The orthogonal perturbation operates on the hidden-state matrix  $J_n \in \mathbb{R}^{Q \times D_{\text{hidden}}}$  ( $D_{\text{hidden}} = 768$  for BERT-base). The truncated SVD in Eq. (17) costs  $\mathcal{O}(Q \cdot D_{\text{hidden}} \cdot r)$  with  $r \ll D_{\text{hidden}}$ , and the subsequent QR decomposition in Eq. (18) is  $\mathcal{O}(r^3)$ . For typical settings (e.g.,  $Q = 100$ ,  $r = 16$ ), this amounts to  $\sim 1.2 \times 10^6$  FLOPs, **three orders of magnitude smaller** than the  $\sim 1.1 \times 10^9$  FLOPs required for a single forward/backward pass of BERT-base on a mini-batch of size 32.
- **Sketching:** The hash-based sketch generation in Eq. (20) involves only integer hash computations and sign operations, with  $\mathcal{O}(Y \cdot Z \cdot D_{\text{hidden}})$  complexity where  $Y \cdot Z \ll D_{\text{hidden}}$ . Empirically, sketching adds  $< 2\%$  to local computation time.

**(ii) Communication-Computation Trade-off Justification.** In edge LLM fine-tuning, **communication latency dominates local computation** due to limited uplink bandwidth and large activation sizes. As shown in Table III, ELSA reduces total communication time by 69.3%–73.7% compared to uncompressed baselines. The marginal increase in local computation ( $< 5\%$  of per-round time) is overwhelmingly offset by the reduction in transmission delay, yielding a **net decrease in end-to-end training time**.

**(iii) Empirical Robustness under Resource Constraints.** If the overhead were excessive, we would observe elevated task failure rates on resource-constrained clients. However, Table V demonstrates that ELSA maintains the **lowest task failure rate** (1.2%) among all evaluated strategies, significantly outperforming static splitting configurations (up to 41.7% failure). This confirms that our resource-aware dynamic splitting (Section III.B.2) successfully accommodates the extra computation without overwhelming device capabilities.

In summary, while ELSA introduces additional computational modules, their overhead is carefully designed to be lightweight, infrequent, or communication-saving. The resulting framework achieves a favorable trade-off: minimal local computation increase for substantial communication reduction and enhanced privacy, ultimately improving system-level efficiency and robustness in heterogeneous edge environments.